PONTIFICIA UNIVERSIDAD CATÓLICA DEL PERÚ

ESCUELA DE POSGRADO

BACKSCATTER COEFFICIENT ESTIMATION USING HIGHLY FOCUSED ULTRASOUND TRANSDUCERS

By

Diego Panizo

Thesis submitted in partial fulfillment of the requirements for the degree of

Master in Digital Signal and Image Processing

in the Graduate School of the Pontificia Universidad Católica del Perú.

Thesis Supervisor: Roberto Lavarello

Examining commitee members:

Paul A. Rodríguez

Benjamín Castañeda

Lima, Perú

September, 2013

Abstract

The backscatter coefficient (BSC) is an intrinsic property that quantifies the amount of energy that is reflected by a material as function of the ultrasound wave frequency. BSCs have been proposed for decades for tissue characterization, along with quantitative ultrasound (QUS) parameters derived from BSCs that have been used to construct images that represent how these properties vary spatially. The availability of formulations based on weakly focusing conditions has resulted in a widespread use of large focal number transducers for BSC estimation. The use of highly focused transducers offers the possibility of improving the spatial resolution of BSC-based imaging. The model by Chen et al. [1] was developed for estimating BSCs using transducers of arbitrary focal number. However, to this date only preliminary experimental validation of this method has been performed.

The goals of the present study are to analyze for the first time the accuracy of Chen's [1] method when estimating BSCs using highly focused transducers through both simulations and experiments, and to analyze the accuracy on the estimation of QUS parameters derived from BSCs (specifically the effective scatterer size (ESD) and concentration (ESC)) applying the Chen et al. [1] model.

To achieve these goals, a theoretical model of BSC synthesis based on the method of Chen et al. [1]. was derived and used with simulated data. The model considers frequency dependent diffraction patterns, and the scatterers in the synthetic data replicate the properties of solid spheres. In experiments, data obtained using highly focused transducers from a physical phantom containing glass beads was used. This experimental data was appropriately compensated for attenuation and transmission effects. The accuracy of Chen's method was evaluated calculating the mean fractional error between the estimated and theoretical BSCs curves for both simulations and experiments. Also, the QUS parameters were estimated and compared with real known parameters. BSCs and QUS parameter estimates were obtained from regions of interest from both the transducer focus and throughout the transducer focal region. Finally, the sound speed and the transducer focus were varied in appropriate ranges when processing the data for the BSC and QUS values estimation in order to assess the robustness of the method to uncertainties in these parameters.

The results showed that BSCs and QUS parameters can be accurately estimated using highly focused transducers if the appropriate model is used, with regions of interest not restricted to be centered at the focus but to the full extension of the -6-dB transducer focal region. It was also verified that well estimated parameters as the sound speed and transducer focus are necessary in order to obtain accurate BSCs and QUS parameters estimates.

Contents

List of Figures

List of Tables

Chapter 1

Introduction

1.1 Background and Context

In many tissue characterization applications it is desirable to obtain information about the microstructure of the material that is being analyzed. The backscatter coefficient (BSC) is an intrinsic property that quantifies the amount of energy that is reflected by a material as function of the ultrasound wave frequency. Many studies in the literature suggest that different materials reflect the ultrasound waves in different ways, therefore, the BSC can be potentially used for tissue characterization. In addition, quantitative ultrasound (QUS) parameters derived from BSCs can be used to construct images that represent how these properties vary spatially in the material. BSCs can be estimated using ultrasound transducers with different focal numbers, the more focused is the transducer, the QUS parameters can be estimated from smaller regions of interest (ROI). Accordingly, the use of highly focused transducers offers the possibility of improving the spatial resolution of BSC-based imaging by reducing the size of the region of interest (ROI) required to estimate BSCs.

In order to obtain meaningful information from BSCs it is necessary to compensate for the ultrasound system dependent properties (transducer diffraction pattern, acoustic-electric response, etc). The availability of methods for estimating BSCs derived from weakly focusing conditions [1, 2] and the extended focal region that results from this conditions [3] has resulted in an overwhelming number of studies that used weakly focused transducers to estimate BSCs from liver [4, 5, 6], breast [7, 8, 9], heart [10, 11] and bones [12] among other organs. Nevertheless, there exist also studies realized using highly focused transducers to obtain QUS parameters derived from BSCs, usually to characterize tissues using high frequency [13, 14, 15, 16]. However, a conclusive study on the accuracy of BSC estimation and derived parameters from properly characterized scattering media using highly focused transducers has not yet been conducted.

The model proposed in [1] provides expressions to estimate BSCs using transducers with arbitrary focal number, and approximate expressions for the case of a weakly focused transducer. Therefore, the use of the expressions in [1] will allow to study the differences in estimating

BSCs with and without assuming weakly focusing conditions from data obtained with highly focused transducers. Some studies available in the literature suggest that the model proposed in [1] may be used to compensate for the transducer diffraction pattern when estimating BSCs from weakly scattering media [17, 18]. However, a conclusive study on the accuracy of BSC estimation and derived parameters from properly characterized and calibrated scattering media using highly focused transducers has not yet been conducted.

1.2 Scope and Objectives

The goals of the present study are (1) to analyze for the first time the accuracy of the model by Chen et al. [1] when estimating BSCs using highly focused transducers through both simulations and experiments, and (2) to analyze the accuracy on the estimation of QUS parameters derived from BSCs (specifically the effective scatterer size (ESD) and concentration (ESC)) applying the model presented in [1].

The specific objectives are to:

1. Develop a theoretical model of BSCs synthesis based on the method of Chen et al. from simulated data that considers frequency dependent diffraction patterns.
2. Analyze through simulations the effectiveness of the Chen et al. method to produce exact BSCs estimates both around the transducer focus and throughout of the transducer focal region.
3. Verify experimentally the accuracy of the BSC estimation using the Chen et al. method.
4. Analyze through simulations the accuracy of the ESDs and ESCs estimates produced using the Chen et al. method to synthesize BSCs around the transducer focus and from side to side of the transducer focal region.
5. Verify experimentally the accuracy of the ESDs and ESCs estimates using the Chen et al. method.
6. Analyze the robustness of the Chen et al. method using focused transducers to parameters with uncertainty like the sound speed and the exact position of the transducer focus.

1.3 Achievements

In this document, the accuracy of the method presented in [1] when estimating BSCs using highly focused transducers through both simulations and experiments were analyzed, along with the accuracy of the estimation of QUS parameters (ESD and ESC) derived from BSCs applying the Chen et al. model. The results clearly showed that BSCs can be accurately estimated using highly focused transducers if the appropriate model is used, with the centers of the regions of

interest not restricted to the transducer focus. The robustness of the method to parameters with uncertainty was also analyzed, and the results showed that even a 1% error in the exact position of the focus or in the sound speed can impair the estimation, being more critical for the case of the ESCs. The results were obtained from both simulated and experimental data. For the simulations a complete model for estimating BSCs using the FIELD II [19] simulation software was developed.

1.4 Overview of the Document

The remainder of this document includes the following chapters:

Chapter 2, Basic Concepts gives a brief description of a focused transducer, the BSC and some relevant equations.

Chapter 3, A Model For BSC Estimation Using FIELD II describes the derivation of a new mathematical model for estimating BSCs using the FIELD II simulation software. Results using weakly and highly focused transducers for estimating BSCs from simulated data are also included in this chapter.

Chapter 4, Accuracy Assessment lists the equations used for estimating BSCs using highly focused transducers from simulated and experimental data. The equations presented to measure the accuracy and the properties of the simulated and experimental transducers are also included. The results obtained using regions of interest centered around the transducer focus and then centered at several positions around the transducer focal region are presented. The accuracy of the method to parameters with uncertainty is also assessed in this chapter.

Chapter 5, Conclusions lists the concluding remarks for this work. All the specific objectives were fulfilled.

Chapter 2

Basic Concepts

2.1 Focused Transducer

A focused transducer has the shape of a spherical cap, and all the points on its surface are equidistant to a point F termed the focal distance. This type of transducer has tipically the peak of the energy of its radiation pattern slightly before the depth F. The geometry of the focused transducer is shown in Fig. 2.1.

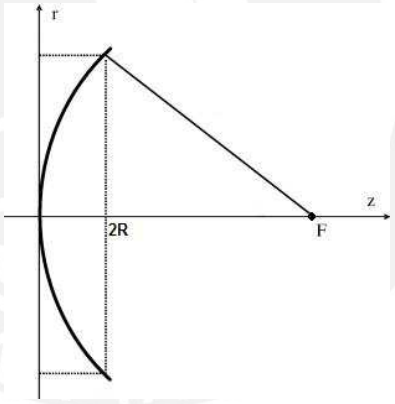

Figure 2.1: Schematic diagram of a focused transducer.

The most important parameter to define a focused transducer is the focal number

$$f/\# = F/2R, \tag{2.1}$$

where R is the transducer radius and $f/\#$ represents a focused transducer with a focal number #. The radiation patter of two focused transducer with different focal numbers are presented in Fig. 2.2.

It can be noticed that when the focal number is lower the focal region become smaller. The axial dimension (A_D) and the lateral dimension (L_D) of the focal region are defined [3] in

equations 2.2 and 2.3 respectively, where λ is the wavelength.

$$A_D = 7.08\lambda f/\#^2. \tag{2.2}$$

$$L_D = 1.028\lambda f/\#. \tag{2.3}$$

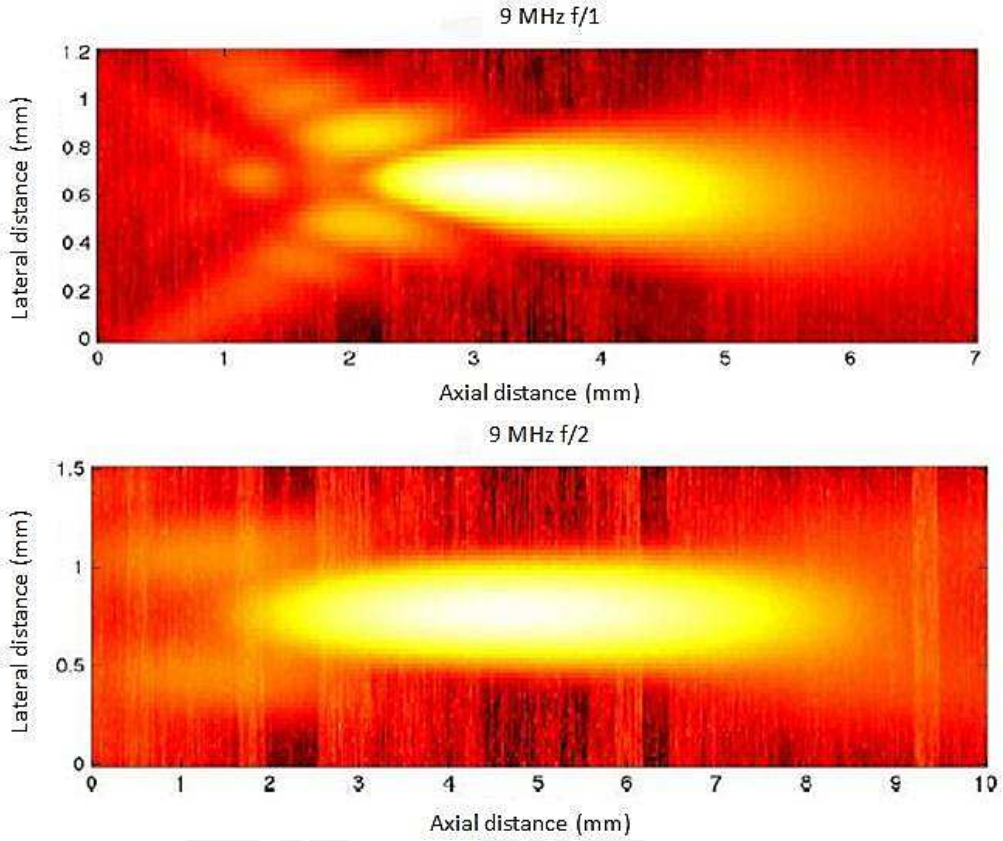

Figure 2.2: Two different radiation patterns. Top 9 MHz f/1 transducer, bottom 9 MHz f/2 transducer. Image courtesy of the University of Illinois

2.2 Backscatter Coefficient

Commonly in ultrasound imaging, radio frequency (RF) data is used to obtain information of structures from hundreds of micrometers to centimeters in scale (structures greater than the acoustic wavelength). Each of the RF signals is a series of echoes backscattered from structures in the interrogation medium. Usually the frequency-dependent information in the RF signals is not used. Instead, the coventional ultrasound imaging relates the envelope of a backscattered RF signal to a gray-scale image.

The ultrasonic backscatter coefficient (BSC) is a useful property for characterizing tissues. It is defined as the differential scattering cross section per unit of volume for a scattering angle

of 180°. The BSC use the frequency-dependent information to characterize different aspects of microstructure in biological tissues. Specifically, BSC has been used to extract the average scatterer sizes and acoustic concentrations (product of the number concentration of scatterers and surrounding tissues) from biological tissues.

Chapter 3

A Model For BSC Estimation Using FIELD II

3.1 Introduction

BSCs are estimated from radio frequency (RF) data that can be obtained both from simulations and experiments. The simulations offer a practical alternative to experiments because acoustics waves can be artificially generated from computer phantoms with their acoustic properties (sound speed, focus position,etc) adjusted to known values. In addition, these properties can be easily changed to other values in case are needed. Many models have been proposed in order to simulate ultrasonic systems for several applications, including BSC estimation. These models may significantly differ in their complexity depending on which wave propagation phenomena are considered (i.e. attenuation, diffraction, multiple scattering, etc). For its simplicity and computational cost, some studies [20, 21] simulated the low radiation pattern as a Gaussian beam (only spatially dependent), for example, to analyze the effects of the cell organization and size distribution on the ultrasound backscatter [20]. To define the optimal axial and lateral resolution,authors in [21] simulated a computer phantom assuming to be acoustically lossless and modeling the emited pulse as a Gaussian beam (laterally). Other studies [22] made use of more complex models based in spectral coherence, statistical analysis or angular compounding.

FIELD II [19] is a free Matlab library created by Jorgen Arendt Jensen in order to simulate a wide variety of ultrasound imaging systems, and it has been previously used in several studies [23, 24]. Two significant features of FIELD II is that it considers the frequency dependent tranasducer diffraction and that it can be directly applied to obtain the rf data needed to estimated the BSCs. On the other hand FIELD II does not consider multiple scattering and propagation in inhomogeneous media. Nevertheless, the combination of the FIELD II simulation software, with a more complete (in comparison to the Gaussian beam model) and efficient (in comparisson to the models that solves the wave equation with finite elements methods) model, that considers the frequency dependent diffraction brings the possibility of obtaining results that are closely

related with real experimental data, along with the benefit of an easily replicable model that can be used in other quantitative ultrasound investigations.

A mathematical model is derived in order to properly simulate an ultrasound system based on the FIELD II simulation software. The properties of the simulated ultrasound system are compensated using a point reference for simplicity and the transducer diffraction correction theory proposed by Chen et al. [1]. BSCs are estimated using the proposed model to assess its reliability.

3.2 Methods

3.2.1 The FIELD II model for a distribution of scatterers

The first step to obtain an equation for the estimation of the BSCs using FIELD II is to calculate the received echo signal from a distribution of scatterers. The equation for the incident pressure at a position $\vec{r}$ can be written as

$$P_{in}(\vec{r};\omega) = P_0(\omega)D_T(\vec{r};\omega), \tag{3.1}$$

where $\omega = 2\pi f$ is the angular frequency of the acoustic wave, $P_0(\omega)$ is the amplitude of the characteristic pressure at the transducer surface and $D_T(\vec{r};\omega)$ is the radiation pattern on transmission (identical to radiation pattern on reception due to recirpocity) defined as

$$D_T(\vec{r};\omega) = D_R(\vec{r};\omega) = \iint_A \frac{e^{-ikr}}{2\pi r}\mathrm{d}A, \tag{3.2}$$

where A is area of the transducer surface and k is the wavenumber. Also, we can define for a single scatterer at a position $\vec{r}$ a scattered pressure,

$$P_S(\vec{r};\omega) = P_{in}(\vec{r};\omega)\frac{e^{-ikr}}{2\pi r}. \tag{3.3}$$

The scattered acoustic pressure received by a transducer due the presence of an isolated scatterer can be expressed as the average of $P_S(\vec{r};\omega)$ over the surface of the transducer, i.e.

$$\bar{P}_S(\vec{r};\omega) = \frac{1}{A}\iint_A P_S(\vec{r};\omega)\mathrm{d}A. \tag{3.4}$$

Replacing eq. (3.3) in (3.4)

$$\bar{P}_S(\vec{r};\omega) = \frac{1}{A}\iint_A P_{in}(\vec{r};\omega)\frac{e^{-ikr}}{2\pi r}\mathrm{d}A. \tag{3.5}$$

And replacing the incident pressure (3.1) in (3.5)

$$\bar{P}_S(\vec{r};\omega) = \frac{1}{A}P_0(\omega)D_T(\vec{r};\omega)\iint_A \frac{e^{-ikr}}{2\pi r}\mathrm{d}A. \tag{3.6}$$

It can be noticed that the last integral in eq. (3.6) is equal to $D_R(\vec{r};\omega)$. Replacing it by its equivalent and making $D_R(\vec{r};\omega) = D_T(\vec{r};\omega) = D(\vec{r};\omega)$, eq. (3.6) can be rewritten as

$$\bar{P}_S(\vec{r};\omega) = \frac{1}{A}P_0(\omega)D^2(\vec{r};\omega). \tag{3.7}$$

Scattered data from an ensamble of N discrete scatterers can be simulated with FIELD II using the function “calc_scat”, which produces the ultrasound waveforms as

$$\bar{P}_S(\vec{r};\omega) = P_0(\omega)\left(\sum_{j=1}^{N}\frac{1}{A}D^2(\vec{r}_j;\omega)\right). \tag{3.8}$$

Then, the effect of an scattering amplitude function that varies with the frequency is added to this echo because it is not considered by the FIELD II program. This can be modeled as

$$\bar{P}_S(\vec{r};\omega) = P_0(\omega)\left(\sum_{j=1}^{N}\frac{1}{A}D^2(\vec{r}_j;\omega)\right)\Lambda(\omega), \tag{3.9}$$

where $\Lambda(\omega)$ is the scattering amplitude function. From this it is possible to obtain the power spectrum from a single data line in a region of interest (ROI), i.e.

$$\left|S_s(\vec{r},k)\right|^2 = |P_0(\omega)|^2\left|\frac{1}{A}\right|^2\left|\sum_{j=1}^{N}D^2(\vec{r}_j;\omega)\sum_{i=1}^{N}D^2(\vec{r}_i;\omega)\right|\times|\Lambda(w)|^2. \tag{3.10}$$

From (3.10) the mean power can be calculated averaging the power spectra of several adjacent data lines and the sum can be reduced following the same criteria as in [1, (17),(18)], obtaining

$$\left\langle\left|S_s(\vec{r},k)\right|^2\right\rangle = |P_0(\omega)|^2\left|\frac{1}{A}\right|^2\sum_{j=1}^{N}\left|D(\vec{r}_j;\omega)\right|^4|\Lambda(w)|^2. \tag{3.11}$$

The last equation will be related with the theoretical BSC in the following subsection.

3.2.2 The theoretical BSC and its relation with the power spectrum of the received echo

The theoretical BSC can be calculated assuming that the analyzed media in consisted by randomly located spherical scatterers, and neglecting coherent and mutiple scattering effects as [2,

(10)]

$$\eta_{th} = \frac{\beta}{4\pi}\int_0^{\infty} p(a)\sigma(k,a)\mathrm{d}a, \tag{3.12}$$
$$\sigma(k,a) = \left|\frac{2}{ka}\Lambda(\omega)\right|^2(\pi a^2),$$

where β is the number of scatterers per unit of volume, $p(a)$ is the estimated scatterer size probability distribution function, and $\sigma(k,a)$ is the backscattering cross-section of an individual scatterer of radius a.

If the particular case of a field with constant size spheres is considered eq. (3.12) is reduced to

$$\eta_{th} = \frac{\beta}{4\pi}\left(\frac{2}{ka}|\Lambda(\omega)|\right)^2\pi a^2. \tag{3.13}$$

Simplifying equation (3.13)

$$\eta_{th} = \beta\frac{1}{k^2}|\Lambda(\omega)|^2\,. \tag{3.14}$$

The last equation for the BSC can be related with the equation (3.11),

$$\left\langle\left|S_s(\vec{r},k)\right|^2\right\rangle = |P_0(\omega)|^2\left|\frac{1}{A}\right|^2\sum_{j=1}^{N}\left|D(\vec{r}_j;\omega)\right|^4\cdot\eta\cdot\frac{k^2}{\beta}. \tag{3.15}$$

Assuming a uniform distribution of scatterers inside the volume of interest and that the received signals are statistically independent, it is possible to change the last sum with an integral times the number of scatterers per unit of volume,

$$\left\langle\left|S_s(\vec{r},k)\right|^2\right\rangle = |P_0(\omega)|^2\left|\frac{1}{A}\right|^2\beta\int_V\left|D(\vec{r};\omega)\right|^4\mathrm{d}V\cdot\eta\cdot\frac{k^2}{\beta}. \tag{3.16}$$

Reordering the terms and simplifying

$$\left\langle\left|S_s(\vec{r},k)\right|^2\right\rangle = |P_0(\omega)|^2\left|\frac{1}{A}\right|^2k^2\int_V\left|D(\vec{r};\omega)\right|^4\mathrm{d}V\cdot\eta. \tag{3.17}$$

The last equation relates the theoretical BSC with the average power spectrum of the received echo.

3.2.3 The FIELD II model for a point reference

The scattered pressure by the reference used for the normalization of the BSC, which consists in a point target located at the geometrical focus F of the transducer, can be modeled as

$$P_{ref}(F;\omega) = \frac{1}{A}P_0(\omega)(D_{ref})^2, \tag{3.18}$$

where

$$D_{ref} = \iint_A \frac{e^{-ikF}}{2\pi F} \mathrm{d}A.$$

The last integral can be numerically evaluated for a concave transducer obtaining

$$D_{ref} = \frac{e^{-ikF}}{2\pi F} \pi (R^2 + d^2).$$

with $d = F\left(1 - \sqrt{1 - \frac{1}{4f/\#^2}}\right)$. And for the case that $R^2 > d^2$

$$D_{ref} \cong \frac{e^{-ikF}}{2\pi F} \pi (R^2). \tag{3.19}$$

Obtaining the power spectrum from the equation (3.18)

$$\left|S_{ref}(\vec{r}, k)\right|^2 = \frac{1}{A^2} \left|P_0(\omega)\right|^2 \left|(D_{ref})^2\right|^2. \tag{3.20}$$

Using equation (3.19) in equation (3.20) and solving for $|P_0(\omega)|^2$,

$$|P_0(\omega)|^2 = \frac{\left|S_{ref}(\vec{r}, k)\right|^2}{\left(\frac{A}{2\pi F}\right)^4} A^2. \tag{3.21}$$

3.2.4 BSC estimation

Using equations (3.17) and (3.21) the backscatter coefficient can be estimated as

$$\eta = \frac{\left\langle \left|S_s(\vec{r}, k)\right|^2 \right\rangle}{\left|S_{ref}(\vec{r}, k)\right|^2} \frac{\left(\frac{A}{2\pi F}\right)^4}{k^2} \frac{1}{\int_V \left|D(\vec{r}; \omega)\right|^4 \mathrm{d}V}. \tag{3.22}$$

For solving the integral in eq. (3.22) two solutions are presented in [1], a general solution (termed here Chen's model - CM) for arbitrary focal number transducers and an approximation (termed here Chen's approximate model - CAM) for weakly focused transducers.

Some modifications have to be done to the equations presented in [1] in order to have consistency between the formulations. Chen [1] defines the mean diffraction correction function as

$$\bar{D}_S(\vec{r}, k) = \frac{1}{\Delta z} \left|\frac{2\pi}{kA}\right|^2 \int_V \left|D_{Chen}(\vec{r}; k)\right|^4 \mathrm{d}V, \tag{3.23}$$

where

$$D_{Chen}(\vec{r}; k) = -ik \iint_S \frac{e^{-ikr}}{2\pi r} \mathrm{d}S,$$

and Δz is the length of the gated region (see Fig. 3.1).

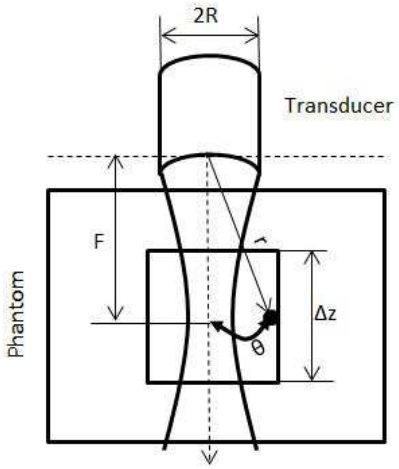

Figure 3.1: Schematic diagram of the geometry.

For the general case Chen et al. gives a solution for eq. (3.23) as

$$\begin{aligned}\bar{D}_S(\vec{r},k) &= \frac{1}{\Delta z}\left|\frac{2\pi}{A}\right|^2 k^2 \int_V \left|\iint_S \frac{e^{-ikr}}{2\pi r}\mathrm{d}S\right|^4 \mathrm{d}V \\ &= \frac{1}{\Delta z}\int_{\bar{r}-\frac{\Delta z}{2}}^{\bar{r}+\frac{\Delta z}{2}} D_S(\vec{r};k)\mathrm{d}r. \end{aligned} \tag{3.24}$$

where $\bar{r}$ is the mean distance from the transducer surface to the sample volume and

$$D_S(\vec{r},k) = \begin{cases} (A/r^2)0.46\exp[-(0.46/\pi)G_P^2(F/r-1)^2], \\ (1+\pi/G_P)^{-1} \le r/F \le (1-\pi/G_P)^{-1}, \\ 1.07(A/r^2)[G_P(F/r-1)]^{-2}, \\ \text{otherwise}, \end{cases} \tag{3.25}$$

where $G_P = (kR^2/2F)$ is the focal gain of the transducer.

From eq. (3.24) the following equality can be obtained

$$\int_V \left|\iint_S \frac{e^{-ikr}}{2\pi r}\mathrm{d}S\right|^4 \mathrm{d}V = \frac{A^3}{(2\pi)^2k^2}\cdot\int_{\bar{r}-\frac{\Delta z}{2}}^{\bar{r}+\frac{\Delta z}{2}} D_S(\vec{r};k)\mathrm{d}r. \tag{3.26}$$

Using the last equality in eq. (3.22) a general solution for estimating BSCs using arbitrary f/# transducers is obtained,

$$\eta_{CM} = \frac{\left\langle\left|S_s(\vec{r},k)\right|^2\right\rangle}{\left|S_{ref}(\vec{r},k)\right|^2}\frac{A}{(2\pi)^2F^4}\cdot\frac{1}{\int_{\bar{r}-\frac{\Delta z}{2}}^{\bar{r}+\frac{\Delta z}{2}} D_S(\vec{r};k)\mathrm{d}r}. \tag{3.27}$$

For the case of weakly focused transducers with small variations over their focal regions, Chen approximated $\bar{D}_S(\vec{r},k)$ as $D_S(\bar{r},k)$. For the specific case when $\bar{r}=F$, the form that solves the integral in equation (3.22) can be written as

$$\int_V \left| \iint_S \frac{e^{-ikr}}{2\pi r} \mathrm{d}S \right|^4 \mathrm{d}V = \frac{A^3 0.46 \Delta z}{(2\pi)^2 F^2 k^2}. \tag{3.28}$$

Using equation (3.28) in (3.22) an approximate solution for estimating BSCs with high f/# transducers when $\bar{r}=F$ is obtained,

$$\eta_{CAMm} = \frac{\left\langle \left| S_s(\vec{r},k) \right|^2 \right\rangle}{\left| S_{ref}(\vec{r},k) \right|^2} \frac{A}{0.46(2\pi)^2 F^2 \Delta z}. \tag{3.29}$$

The termin CAM will be used for the general case ($\bar{r} \neq F$).

3.2.5 The spatial gated region

In order to appropriately delimit the gated region to be used, the idea of the ”Spatial Receive Gate” presented in [1, Appendix A] is applied. Due to the finite pulse duration the spatially gated signal will contain information that can be partially or fully received depending on its source inside or outside of the gated region. In Fig. 3.2 the diagram of the spatial gated region is presented. The information coming from the region [r1,r2-PL] (PL is the length of the pulse) will be fully received, and the information coming from the regions [r1-PL,r1[and]r2-PL,r2] will be partially received. With this information an spatial receive gate function $G(r)$ can be defined as,

$$G(r) = \begin{cases} r/PL + (1 - r1/PL), & r1 - PL \leq r < r1 \\ 1, & r1 \leq r \leq r2 - PL, \\ -r/PL + r2/PL, & r2 - PL < r \leq r2 \\ 0, & \text{otherwise}, \end{cases} \tag{3.30}$$

where r1 and r2 are the distances from the transducer to the beginning and to the end of the gate respectively. This function is used along with the diffraction correction function as a more practical and accurate way to delimit the receive gate. $G(r)$ is used by redefining $\xi(k,r)$ as

$$\xi(k,\vec{r}) = \int_{\bar{r}-\frac{\Delta z}{2}}^{\bar{r}+\frac{\Delta z}{2}} G(r) D_S(\vec{r};k) \mathrm{d}r \tag{3.31}$$

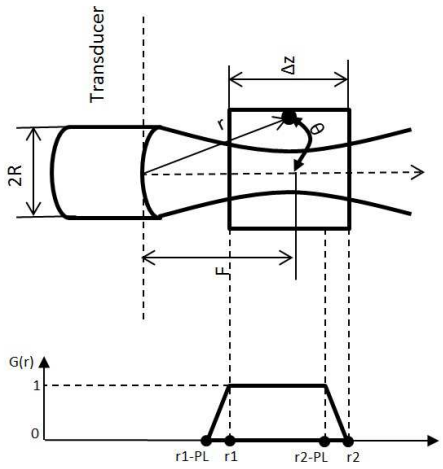

Figure 3.2: Diagram of the spatial gated region.

3.3 Results

3.3.1 Scattering amplitude function

For all the simulations, the solid sphere model described by Faran [25] (Eq. (31) with the corrections to Eq. (30) noted by Hickling [26]) is used for replacing the scattering amplitude function $\Lambda(\omega)$.

$$\Lambda(\omega) = \sum_{m=0}^{\infty}(-1)^m(2m+1)sin(\Upsilon_m)exp(i\Upsilon_m), \tag{3.32}$$

where,

$$\begin{aligned}
\Upsilon_m &= tan^{-1}\left(tan\delta_m(ka)\frac{[tan\Phi_m + tan\alpha_m(ka)]}{tan\Phi_m + tan\beta_m(ka)}\right), \\
\delta_m(x) &= tan^{-1}\left[-j_m(x)/n_m(x)\right], \\
\alpha_m(x) &= tan^{-1}\left[-xj'_m(x)/j_m(x)\right], \\
\beta_m(x) &= tan^{-1}\left[-xn'_m(x)/n_m(x)\right], \\
\Phi_m &= tan^{-1}\left[(\rho/\rho_1)tan\zeta_m(k_1a,\sigma)\right],
\end{aligned} \tag{3.33}$$

$$\zeta_m(k_1a,\sigma) = tan^{-1}\left[-\frac{k_2^2a}{2}\frac{\frac{k_1aj'_m(k_1a)}{k_1aj'_m(k_1a)-j_m(k_1a)} - \frac{2(m^2+m)j_m(k_2a)}{(m^2+m-2)j_m(k_2a)+k_2^2aj''_m(k_2a)}}{\frac{k_1^2a\{[\sigma/(1-2\sigma)]j_m(k_1a)-j''_m(k_1a)\}}{k_1aj'_m(k_1a)-j_m(k_1a)} - \frac{2(m^2+m)[j_m(k_2a)-k_2aj'_m(k_2a)]}{(m^2+m-2)j_m(k_2a)+k_2^2aj''_m(k_2a)}}\right],$$

where ζ_m is the scattering phase angle, j_m is the spheric bessel function, n_m is the spheric neumann function, k_1 is the wavenumber for the compressional waves inside the sphere, k_2 is the wavenumber for the shear waves inside the sphere, a is the sphere radius and σ is the poisson's ratio.

3.3.1.1 Model evaluation

In order to assess the reliability of the model, several simulations were conducted for different weakly focused transducers to obtain BSC estimates using the CAM and compare them with the theoretical results. The simulated phantom contained 41μm diameter solid spheres and attenuation effects were not included. In all the simulations the gated region was centered around the transducer focus. For all the cases the gated region was selected to have a length of 15 wavelengths [21]. The results are presented in Fig. 3.3.

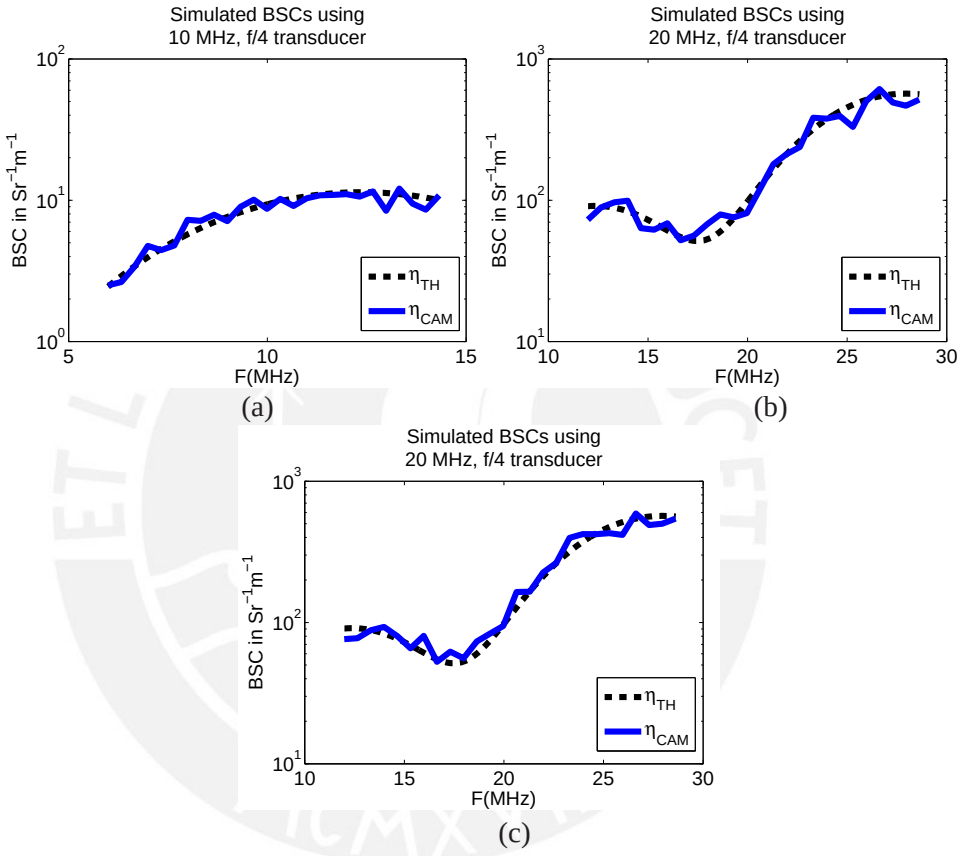

Figure 3.3: BSC estimates using CAM (solid) and theoretical BSC (dash) for three different transducers. From the left to the right, f_0=10MHz, $f/\#$=4 and 0.5"diameter; f_0=20MHz, $f/\#$=4 and 0.5"diameter; f_0=20MHz, $f/\#$=4 and 0.25"diameter.

The results show great correlation between the theoretical and estimated BSCs when using weakly focused transducers with the CAM solution. The mean fractional error (MFE) was calculated between the theoretical and estimated BSCs as

$$MFE = \frac{1}{N}\sum_{i=1}^{N}\frac{|(\eta(k_i) - \eta_{th}(k_i))|}{\eta(k_i)} * 100, \tag{3.34}$$

and the results are presented in Table 3.1. along with the transducers properties.

Table 3.1: Transducers used to obtain the simulated data

f_0(MHz)	$f/\#$	Diameter	Analyzis bandwith (MHz)	MFE (%)
10	4	0.5 in	[6-14]	9.1
20	4	0.5 in	[12-28]	11.1
20	4	0.25 in	[12-28]	12.2

The MFE values support what is observed on Fig. 3.3. For weakly focused transducers MFE of less than 12.2% is obtained proving the reliability of the model. It also can be observed that the MFE value is lower for low frequencies, this occurs because the shape of the theoretical BSC curves is smoother for low frequencies.

3.3.1.2 Approximate vs. General solution

To assess the robustness of the general solution (CM) when estimating BSCs using highly focused transducers, several simulations were made and the results were compared to the estimates using the approximate solution (CAM) and the theoretical curves. The results are presented in Fig. 3.4. These results clearly show that for the case of highly focused transducers the general solution gives better estimates than the ones produced by CAM. An improvement of around 20% is obtained for both f/1.5 transducers, and around 4% for the f/2 transducer.. The MFE was calculated and the results are presented in Table 3.2. along with the transducers properties.

Table 3.2: Highly focused transducers used to obtain the simulated data

f_0(MHz)	$f\#$	Diameter	Analyzis bandwith (MHz)	MFE (CAM) (%)	MFE (CM) (%)
10	1.5	1 in	[6-14]	30.1	9.5
10	2	1 in	[6-14]	11.4	7.3
15	1.5	0.5 in	[9-21]	30.4	9.6

3.4 Summary

A mathematical model for estimating absolute BSC vs. frequency curves using FIELD II was derived. The model was verified against theoretical BSC curves showing great matching between them.

Two specific solutions to the diffraction correction function were given based in the study of Chen et al. and these solutions were used to obtain equations for estimating BSCs for the case of weakly focused transducers (CAM) and for the general case of arbitrary focal number transducers (CM).

The results with the simulated transducers shown that the CM gives much better results than the ones obtained using CAM when using highly focused transducers. These preliminary

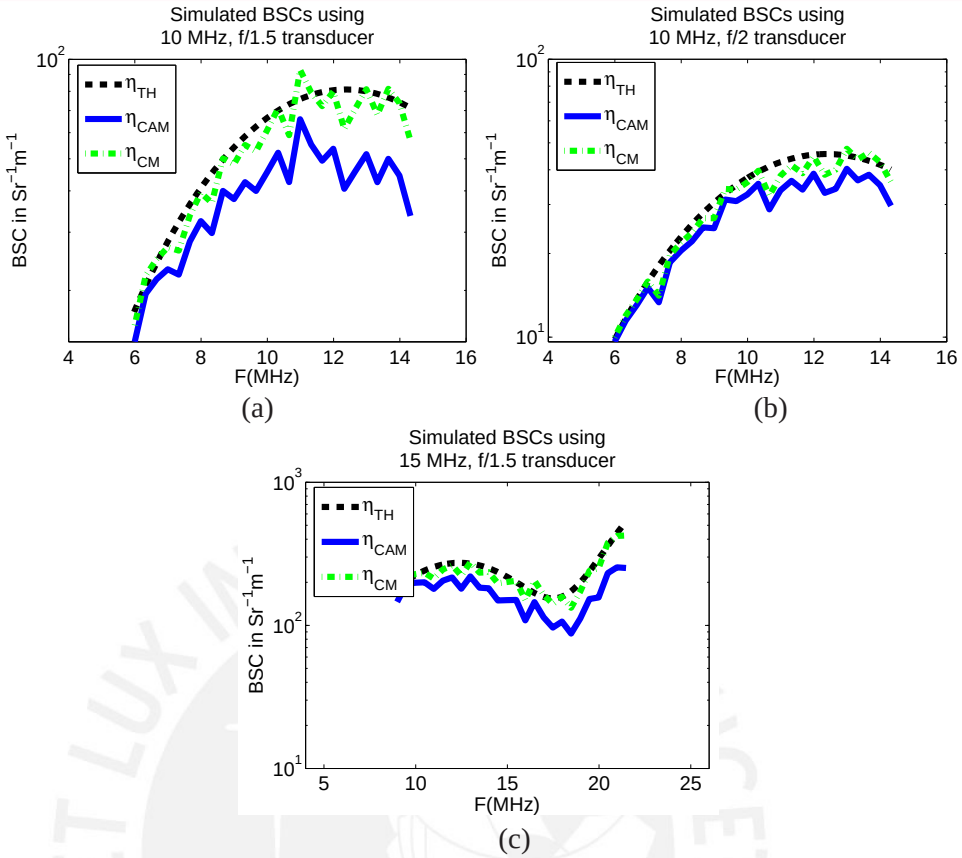

Figure 3.4: BSC estimates using the CAM (solid) and CM (dot-dash) solutions three highly focused transducers ((a) corresponds to a transducer with f_0=10 MHz, $f/\#$=1.5 and 1"diameter, (b) corresponds to a transducer with f_0=10 MHz, $f/\#$=2 and 1"diameter, and (c) corresponds to a transducer with f_0=15 MHz, $f/\#$=1.5 and 0.5"diameter).

results support the use of the presented model with experimental data obtained using highly focused transducers.

Chapter 4

Accuracy Assessment

4.1 Introduction

The model proposed in [1] provides expressions to estimate BSCs using transducers with arbitrary focal number, and approximate expressions for the case of a weakly focused transducer. Therefore, the use of the models in [1] will allow us to study the differences between estimating BSCs with and without assuming weakly focusing conditions from data obtained with highly focused transducers. Some studies available in the literature suggest that the model proposed in [1] may appropriately compensate diffraction effects when estimating BSCs from weakly scattering media. Some of them make use of the expressions for weakly focused transducers, with data obtained from calibrated phantoms as in [27] (with an f/2 transducer) and in [28] (with an f/8 transducer). In [18] BSCs were not estimated but the diffraction curves presented by Chen were compared against the power spectrum of the backscattered signal as a function of depth, but is suggested that the curves have better correlation at low frequencies. The data were obtained from human dermis. In [29] and in [30] BSCs were estimated from non-calibrated imaging targets (human tissues). Despite these works, a conclusive study on the accuracy of BSC estimation and derived parameters from properly characterized scattering media using highly focused transducers has not yet been conducted and this is the limitation that this work is intended to redress.

The goal of the present study is (1) to analyze for the first time the accuracy of the model by Chen et al. when estimating BSCs using highly focused transducers through both simulations and experiments, and (2) to analyze the accuracy on the estimation of QUS parameters derived from BSCs (specifically the effective scatterer size (ESD) and the effective scatterer concentration (ESC)) applying the Chen et al. model.

In Chapter 3 a model for estimating BSCs using the FIELD II [19] simulation software that includes the frequency dependent diffraction effects was derived. The model gives the possibility of using any formulation for the diffraction compensation. Because of this, the formulations proposed in [1] for the diffraction compensation can be directly used to estimate BSCs and QUS parameters from simulated data. This data can be obtained using weakly or highly focused

transducers. In addition, the model can use any scattering function, so a computer phantom that is comparable with a real phantom can be simulated.

The simulations were used to analyze the accuracy of Chen's model when estimating BSCs and QUS parameters throughout the focal region and not just at the transducer focus in order to assess its applicability in QUS imaging. The experimental data were used to verify the simulation results.

The robustness of the model to uncertainties in parameters like the sound speed and exact position of the focus was verified. A physical phantom with an independently calibrated BSC was used.

The next section briefly describes the methods used for the BSCs and the QUS parameter estimation for both simulations and experiments. In Section 4.3 the results are presented. The conclusions of the present Chapter are presented in Section 4.4.

4.2 Methods

4.2.1 Experimental BSC estimation with a reference plate

4.2.1.1 Chen's model (CM) with a planar reference

In experiments, the reference spectrum $\left|S_{ref}(\vec{r},k)\right|^2$ was obtained from a planar reflector with pressure reflection coefficient γ located at depth F. For experimental data BSCs can be estimated as (Ref [1], Eqs. (31), (34), (52) and (57))

$$\eta(k,\vec{r}) = \frac{\left\langle\left|S_s(\vec{r},k)\right|^2\right\rangle}{\left|S_{ref}(\vec{r},k)\right|^2}\frac{\gamma^2}{A}D_{ref}(F,k)H(k)\cdot\frac{1}{\int_{\bar{r}-\frac{\Delta z}{2}}^{\bar{r}+\frac{\Delta z}{2}} D_S(\vec{r};k)\mathrm{d}r}, \tag{4.1}$$

$$D_{ref}(F,k) = |\exp(-iG_P)[J_0(G_P)+iJ_1(G_P)]-1|^2,$$

where $H(k)$ is a function that compensates for attenuation effects (Ref. [31], Eq. (16)) and $J_m(.)$ is the m-th order Bessel function.

4.2.1.2 Chen's approximate model (CAM) with a planar reference

An approximate model to estimate BSCs using weakly focused transducers was also provided in [1]. Using this approximate model BSCs can be estimated as (Ref [1], Eqs. (31), (54) and (57))

$$\eta(k,\vec{r}) = \frac{\left\langle\left|S_s(\vec{r},k)\right|^2\right\rangle}{\left|S_{ref}(\vec{r},k)\right|^2}\frac{\gamma^2}{D_s(\bar{r},k)\Delta z}D_{ref}(F,k)H(k). \tag{4.2}$$

It can be noticed that the only difference between CM and CAM is the integration of D_s throughout the gated region.

4.2.2 Simulated and experimental data

4.2.2.1 Simulated data

In simulations, BSC estimates were obtained from a simulated phantom containing 41 μm diameter solid spheres. In particular, the model of Faran [25] as presented in (3.30) was used to replace $\Lambda(w)$. Attenuation effects were not included. The properties of the simulated transducers are given in Table 4.1.

Table 4.1: Transducers used to obtain the simulated data

Simulated Transducers			
f_0(MHz)	$f/\#$	Diameter	ka
10	1.5	0.5 in	[0.52-1.24]
10	2	1 in	[0.52-1.24]
10	3	0.5 in	[0.52-1.24]

4.2.2.2 Experimental data

In physical experiments, rf data were obtained from an agar physical phantom containing glass beads of 41+/-5 μm diameter. The attenuation coefficient was measured independently using an insertion loss technique in through transmission. The reference was a Plexiglass planar reflector ($\gamma = 0.37$). The properties of the experimental transducers are given in Table 4.2.

Table 4.2: Transducers used to obtain the experimental data

Experimental Transducers			
f_0(MHz)	$f/\#$	Diameter	ka
10	1.5	0.5 in	[0.44-1.09]
10	2	1 in	[0.44-1.09]
10	3	0.5 in	[0.65-1.26]

The 10 MHz experimental transducers were used due their availability and in order to have a fixed ka range for different f/# transducers. The properties of the simulated transducers were based on the experimental transducers for an straightforward comparison.

4.2.3 BSC parameter estimation

Accuracy was quantified using the mean fractional error (MFE) between the estimated and theoretical BSC curves as defined in (3.34). BSCs were estimated using gate lengths (Δz) between 15λ and 30λ. Variance effects were reduced by using data from 441 rf lines.

QUS parameters were also obtained from the estimated BSCs. ESD estimates were obtained by solving the optimization problem

$$ESD = 2 \arg\min_{a} \frac{1}{N} \sum_{i=1}^{N} \left[X(\eta(k_i), \sigma(k_i, a)) - \bar{X} \right]^2, \tag{4.3}$$

$$X(r, s) = 10 \log_{10}(r/s), \tag{4.4}$$

where $\bar{X}$ is the mean value of $X(\eta(k_i), \sigma(k_i, a))$ within the analysis wave number bandwidth $k_i \in [k_{min}, k_{max}]$. Once an estimate of the ESD has been calcutaled, the ESC can be estimated as

$$ESC = 4\pi \frac{\sum_{i=1}^{N} \eta(k_i), \sigma(k_i, ESD/2)}{\sum_{i=1}^{N} \sigma^2(k_i, ESD/2)}. \tag{4.5}$$

The accuracy between the estimated and actual ESD value was quantified using the fractional error (FE) as

$$FE(x) = \frac{(x - x_{th})}{x} * 100. \tag{4.6}$$

The accuracy between the estimated and actual ESC value was quantified using a decibel scale ($10 \log_{10}(ESC/\beta)$).

4.3 Results

4.3.1 Around the transducer focus

The MFE was calculated for both, simulated and experimental data collected from gated regions centered at the transducer focus. These results are reported in Table 4.3. The simulation results suggest that the CAM MFE increases with increasing Δz for highly focused transducers ($f/\#<3$), with MFEs exceeding 50% for the 10 MHz, f/1.5 transducer. This result is expected due to the size of the -6-dB focal region of a focused circular piston (eq. (2.2)), and therefore diffraction effects across a given distance are more significant for lower f/#s values. For example, for a f/1.5 transducer the focal region is approximately 15.75λ and therefore the use of Δz values of 15λ or 30λ implies that the ROI covers the full extension of the focal region or further. In contrast, the use of CM results in MFE values that were highly insensitive to Δz (i.e. variations of less than 2.3% for Δz values between 15λ and 30λ) for all focal numbers considered in the simulations. Moreover, in some cases the MFEs were largely reduced when using the CM instead of the CAM, with values below 10% for all the simulated cases and more of than a fourfold increase in accuracy observed both with the f/1.5 and f/2 transducers for $\Delta z = 30\lambda$.

The improvements in BSC estimation accuracy were much more evident when highly focused transducers were used, but the results with the simulated and experimental f/3 transducers suggest that CM may also provide minor improvements when using weakly focused transducers compared to methods based on weakly focusing approximations such as the CAM.

Table 4.3: MFE in simulations and experiments

MFE in Simulations				
Transducer	CAM ($\Delta z = 15\lambda$)	CAM ($\Delta z = 30\lambda$)	CM ($\Delta z = 15\lambda$)	CM ($\Delta z = 30\lambda$)
10 MHz f/1.5	30.4%	57.1%	9.5%	10.0%
10 MHz f/2	14.6%	34.9%	6.8%	8.1%
10 MHz f/3	8.8%	8.2%	8.7%	6.4%
MFE in Experiments				
Transducer	CAM ($\Delta z = 15\lambda$)	CAM ($\Delta z = 30\lambda$)	CM ($\Delta z = 15\lambda$)	CM ($\Delta z = 30\lambda$)
10 MHz f/1.5	20.5%	46.0%	5.7%	5.2%
10 MHz f/2	7.3%	22.4%	4.8%	5.1%
10 MHz f/3	19.8%	23.1%	18.2%	17.1%

It can also be observed that although the experimental results support the significant reduction on MFE when using the CM instead of the CAM, the MFE for the 10 MHz f/3 transducer was larger than expected. Potential reasons for this discrepancy may include errors in modeling the transducer geometry, errors in the assumed theoretical BSC, and noise effects. Regardless, the results support advocating for the use of CM when estimating BSCs instead of the CAM for highly focused transducers.

Figure 4.1 shows the experimental BSC curves produced with all the 10 MHz experimental transducers using the CM and the CAM for $\Delta z = 15\lambda$ and $\Delta z = 30\lambda$. It can be observed that all the estimated BSC curves are closer to the theoretical ones after using the appropriate correction (i.e., the CM), which is consistent with the MFE values reported in Table 4.3.

Although the choice of large Δz values allowed to analyze the ability of both CM and CAM to correct for depth-dependent diffraction effects, the choice of gate lengths as large as 30λ is not consistent with the goal of constructing high resolution quantitative ultrasound images. Therefore, a similar analysis using shorter ROIs centered at several depths along the transducer focal region was also conducted.

4.3.2 Assessment of the estimation method along the transducer focal region

Based on the results of the previous section, it is expected that CM will outperform CAM for the general scenario where $r \neq F$. In order to verify the difference between the CM and its approximations when estimating BSCs using ROIs throughout the transducer focal region, a simulation and an experiment were conducted.

The CM as presented in (3.27) and (4.1) were used for the simulation and the experiment respectively, and the CAM as presented in (3.28, 3.22) and (4.2) were used for the simulation and the experiment respectively. In addition, two modified versions of the CAM, called CAMm

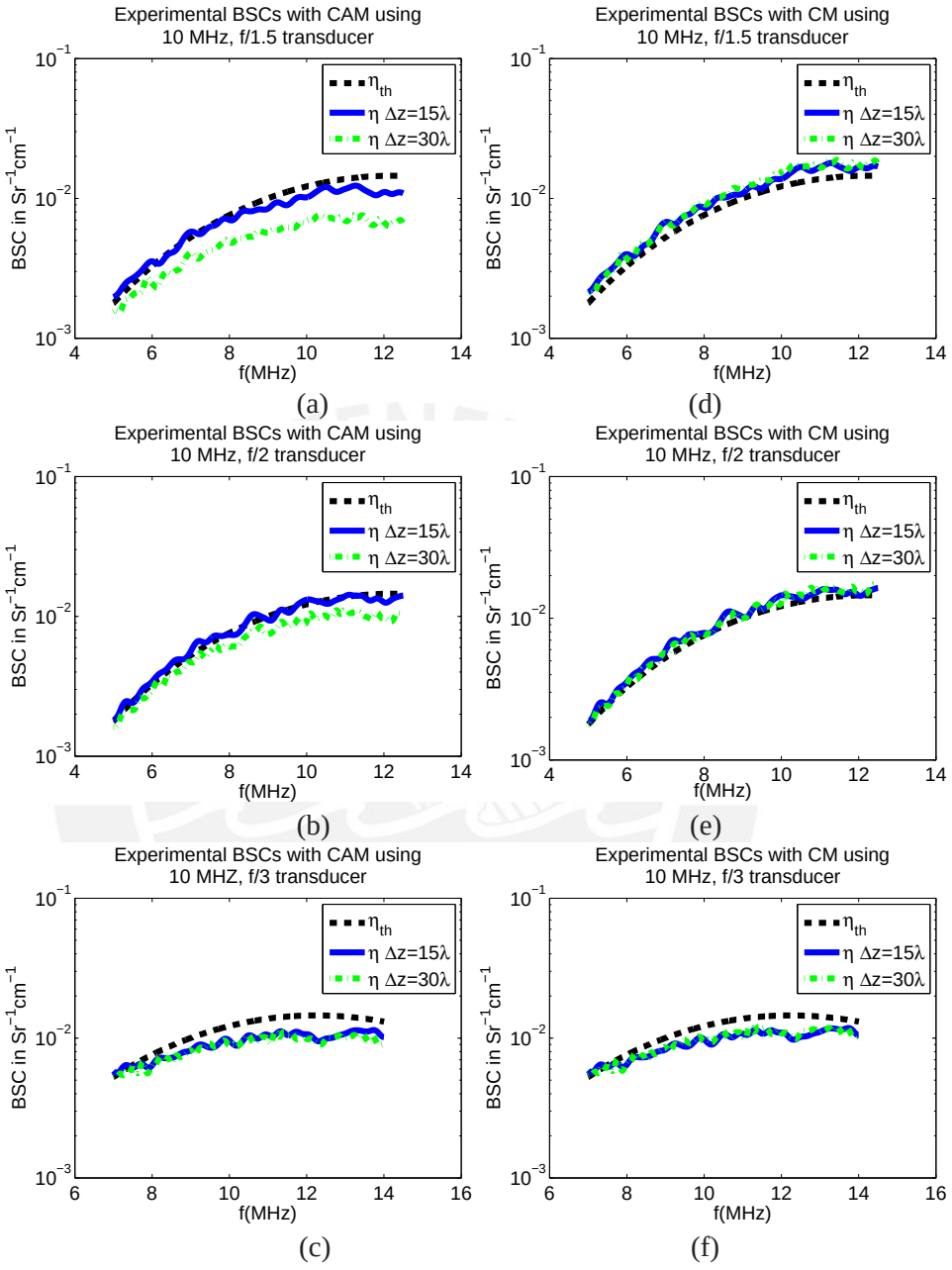

Figure 4.1: BSCs estimates with 15 and 30 wavelengths gated regions and theoretical BSCs (dotted line) for three experimental highly focused transducers ((a) and (d) corresponds to a transducer with f_0=10 MHz, $f/\#$=1.5 and 0.5"diameter, (b) and (e) corresponds to a transducer with f_0=10 MHz, $f/\#$=2 and 1"diameter, (c) and (f) corresponds to a transducer with f_0=10 MHz, $f/\#$=3 and 1"diameter). The first three estimates (top) were obtained using CAM and the second three (bottom) were obtained using CM.

(modified CAM), assuming $\bar{r} = F$ as presented in equation (3.29) for a point reference, and as

$$\eta(k,\vec{r}) = \frac{\left\langle \left|S_s(\vec{r},k)\right|^2 \right\rangle}{\left|S_{ref}(\vec{r},k)\right|^2} \frac{2.17F^2\gamma^2}{A\Delta z} D_{ref}(F,k)H(k). \tag{4.7}$$

for a planar reference were used to explore the performance of the method to a naive approximation.

Gated regions of $\Delta z = 15\lambda$ [21] centered at several positions along the transducer -6-dB focal region (from side to side) were used. The BSC and the QUS parameters were estimated from all the gated regions, and the errors in estimating BSCs, ESDs, and ESCs for all the estimations. A 10 MHz, f/2 and 0.5" diameter transducer was used for both, the simulation and the experiment. The simulation and the experimental results are presented in Figs. 4.2 and 4.3, respectively.

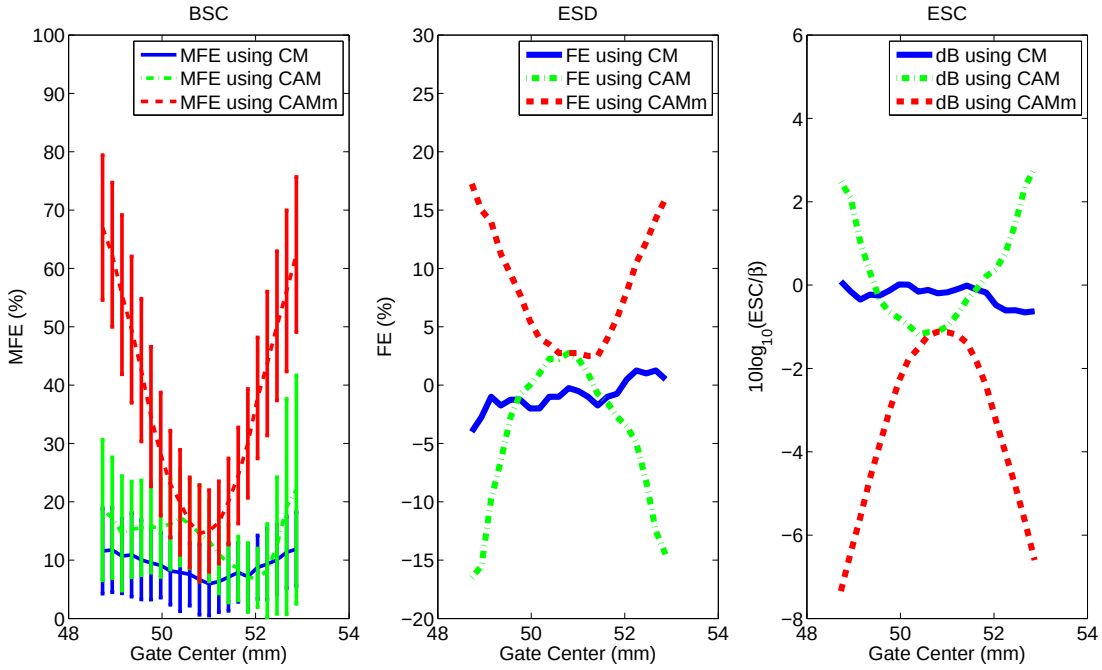

Figure 4.2: Simulation results of the BSC MFE and ESD/ESC FEs for the 10 MHz, f/2 transducer. Three methods were used to estimate the BSCs, the CAMm (dash), the CAM (dot-dash) and the CM (solid).

The results clearly show for both, the simulation and the experiment, that the general method (CM) for estimating BSCs gives better results throughout the transducer focal region than the approximate method (CAM) and its modified version (CAMm) as expected. It can be observed that the BSC MFE and the ESC FE were reduced when using the CM while moving away from the transducer focus. In simulations, a 27% and a 5% improvement in the average MFE for the BSC estimation can be observed when using CM instead of CAMm and CAM respectively. In experiments, a 10% and a 0.5% improvement in the average MFE for the BSC

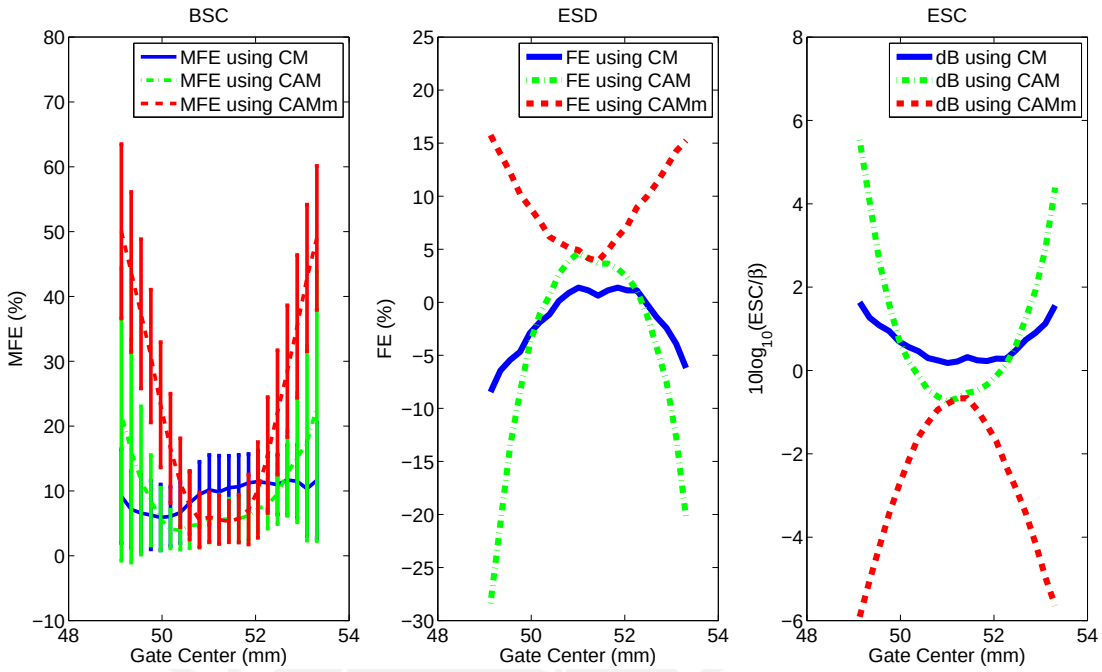

Figure 4.3: Experimental results of the BSC MFE and ESD/ESC FEs for the 10 MHz, f/2 transducer. Three methods were used to estimate the BSCs, the CAMm (dash), the CAM (dot-dash) and the CM (solid).

estimation can be observed when using CM instead of CAMm and CAM respectively. In addition, a slightly lower improvement can be noticed in the ESD FE for both, simulations and experiments when using the CM. The average error for the BSC, ESD and ESC throughout the focal region for the CM and its approximations are presented in Table 4.4. Even though the average MFE does not show a big reduction in Table 4.4., Figs. 4.2 and 4.3 clearly show that the MFE increases when moving away from the transducer focus.

Table 4.4: Average error in simulations and experiments

Average error in simulations			
Method	Average BSC error (%)	Average ESD error (%)	Average ESC error (dB)
CM	9.0%	-0.9%	-0.2 dB
CAM	14.0%	-4.2%	0.3 dB
CAMm	36.7%	8.2%	-3.4 dB
Average error in experiments			
Method	Average BSC error (%)	Average ESD error (%)	Average ESC error (dB)
CM	11.5%	-2.5%	0.8 dB
CAM	12.0%	-5.3%	1.2 dB
CAMm	21.7%	8.5%	-2.6 dB

In order to visually assess the improvement of the CM versus the CAMm, QUS images

presenting the ESD and ESC fractional errors from a computer phantom using the 10 MHz, f/2 transducer are presented in Fig. 4.4.

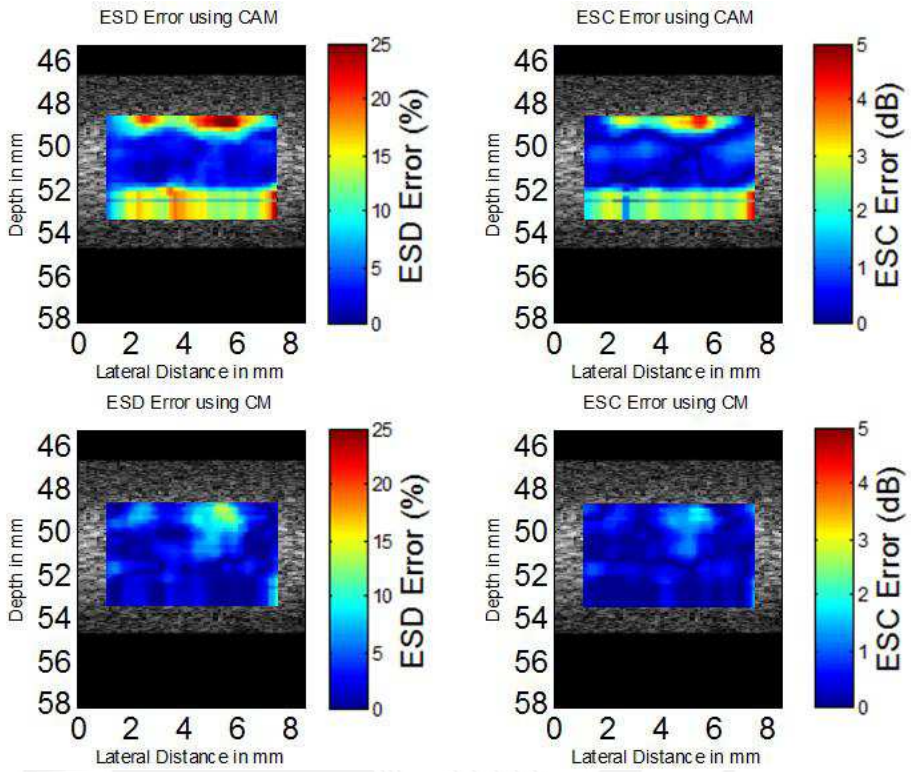

Figure 4.4: Simulated QUS images showing the ESD and the ESC absolute estimation error, both with the CM and CAMm for the 10 MHz, f/2 transducer. The estimates were made using gated regions of 15 wavelengths and 15 adjacent scan lines along all the focal region.

These results clearly show that the CM gives quantitatively much better results than its approximations throughout the transducer focal region. Based on this, just the CM will be used for estimating the BSCs in the following sections.

4.3.3 Simulations along the transducer focal region

New simulations were made using gated regions of 15λ centered at several positions throughout the transducer -6-dB focal region. The BSC and the QUS parameters were estimated from all the gated regions, and the MFE and the FE were calculated for all the estimations. Unfortunately, some parameters that are required by the method by Chen et al. may not be known exactly. For example, the sound speed tends to vary slightly in soft tissues [32], being the extremes the fat and muscle. On the other hand, ultrasound transducers manufacturers usually give margins of error with respect to the exact position of the focus. To assess the robustness of the method to parameters with uncertainty, BSCs were estimated from simulated data generated using the 10 MHz transducers with the properties given in Table 4.1 with a sound speed of 1480m/s but assuming a different sound speed and focal depth. The deviation between the given and

assumed values for the focus position and for the sound speed was chosen to be from about 1% in order to assess the robustness against really small deviations. The results for the simulated transducers assuming different focal depths are presented in Figs. 4.5-4.7.

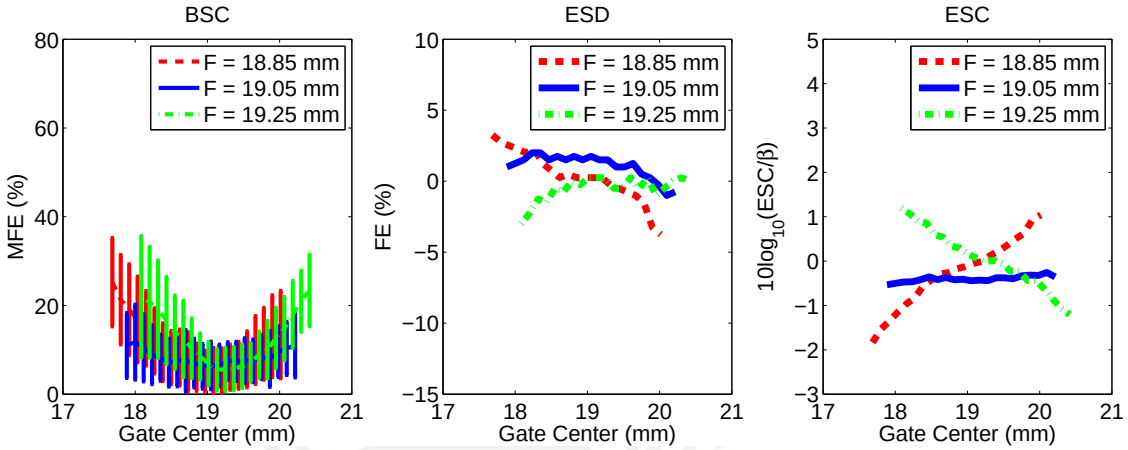

Figure 4.5: Simulation results of the BSC MFE and ESD/ESC FEs for the 10 MHz, f/1.5 transducer with a 19.05 mm focus. The focus assumed when calculating the BSCs was set to 18.85 mm (dash), 19.05 mm (solid) and 19.25 mm (dash-dot) in order to assess the robustness of the method.

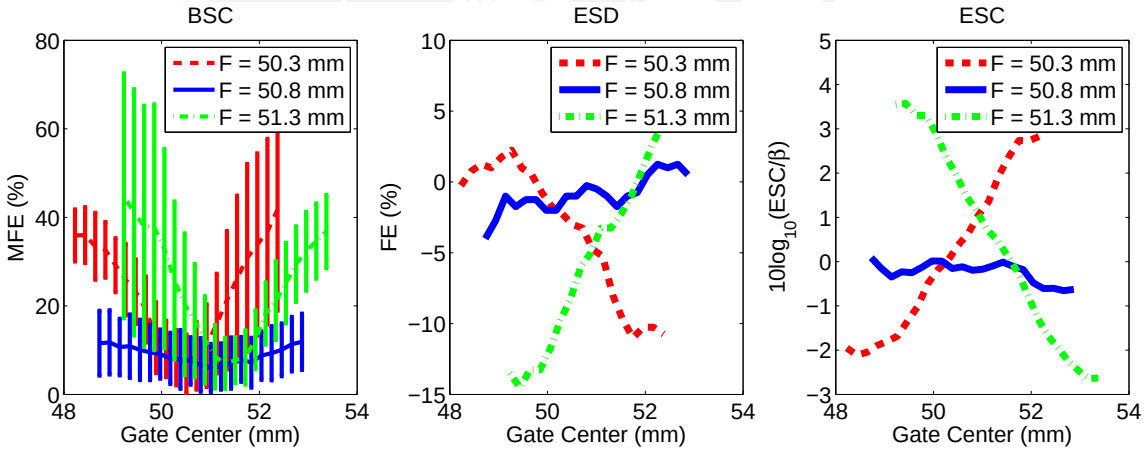

Figure 4.6: Simulation results of the BSC MFE and ESD/ESC FEs for the 10 MHz, f/2 transducer with a 50.8 mm focus. The focus assumed when calculating the BSCs was set to 50.3 mm (dash), 50.8 mm (solid) and 51.3 mm (dash-dot) in order to assess the robustness of the method.

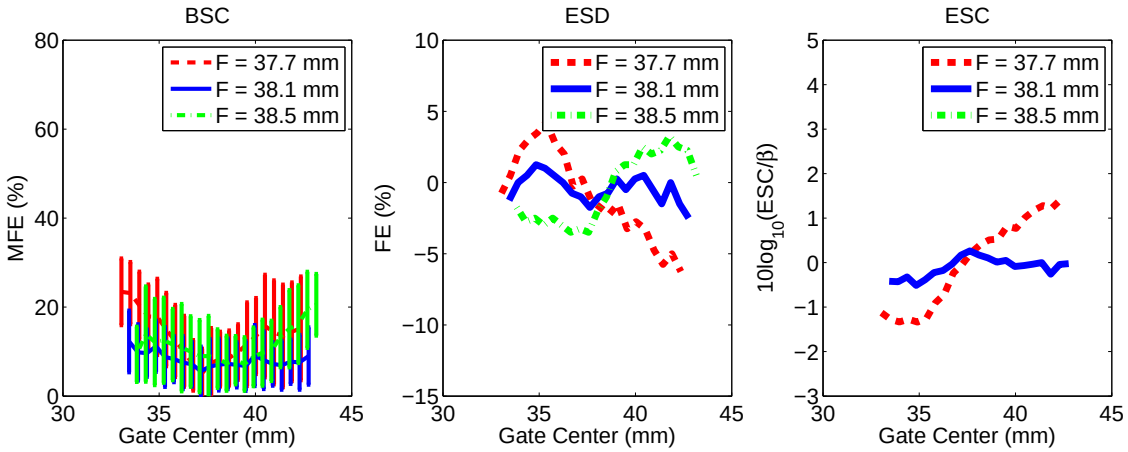

Figure 4.7: Simulation results of the BSC MFE and ESD/ESC FEs for the 10 MHz, f/3 transducer with a 38.1 mm focus. The focus assumed when calculating the BSCs was set to 37.7 mm (dash), 38.1 mm (solid) and 38.5 mm (dash-dot) in order to assess the robustness of the method.

The results for the 10 MHz simulated transducers, but now assuming different sound speeds are presented in Figs. 4.8-4.10.

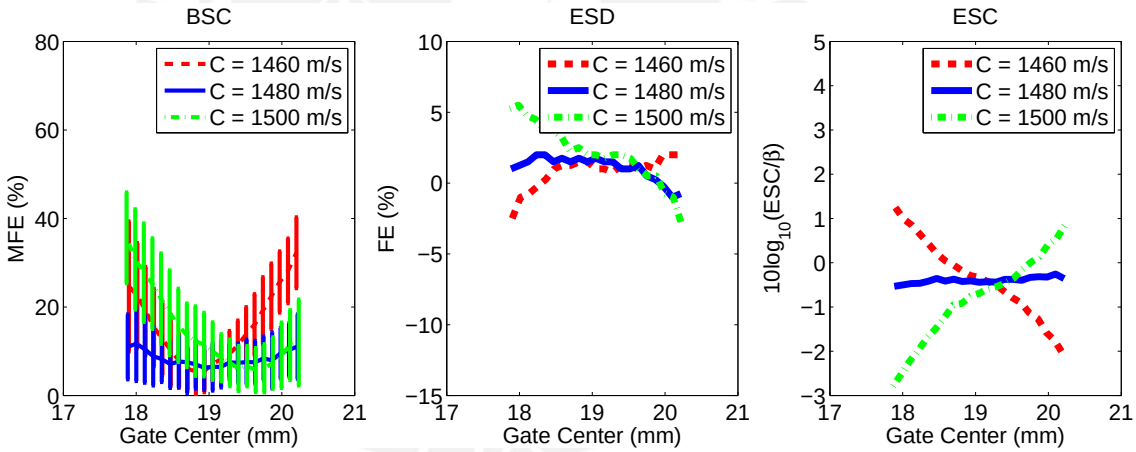

Figure 4.8: Simulation results of the BSC MFE and ESD/ESC FEs for the 10 MHz, f/1.5 transducer with a 1480 m/s sound speed. The sound speed assumed when calculating the BSCs was set to 1460 m/s (dash), 1480 m/s (solid) and 1500 m/s(dash-dot) in order to assess the robustness of the method.

It can be observed that although on the average the CM provides accurate QUS estimates, the performance of the CM may degrade significantly when the assumed focus location is off even by 1% of its true value. The same behavior can be observed with the sound speed. Nevertheless, results with lower errors can be obtained if the mismatch in these parameters is less than 1%, especially for ESCs, even with f/1.5 transducers.

The results shown in Figs. 4.5-4.10, besides showing the behavior described before, exhibit another interesting behavior that can be more appreciable for the ESCs. It can be observed that when the assumed focus position is before or after the real focus, the ESCs estimates have a

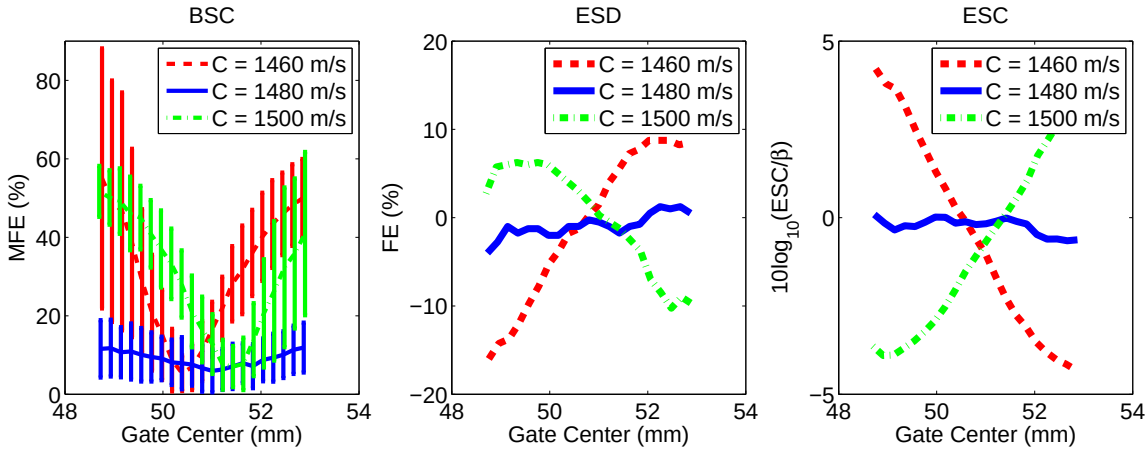

Figure 4.9: Simulation results of the BSC MFE and ESD/ESC FEs for the 10 MHz, f/2 transducer with a 1480 m/s sound speed. The sound speed assumed when calculating the BSCs was set to 1460 m/s (dash), 1480 m/s (solid) and 1500 m/s(dash-dot) in order to assess the robustness of the method.

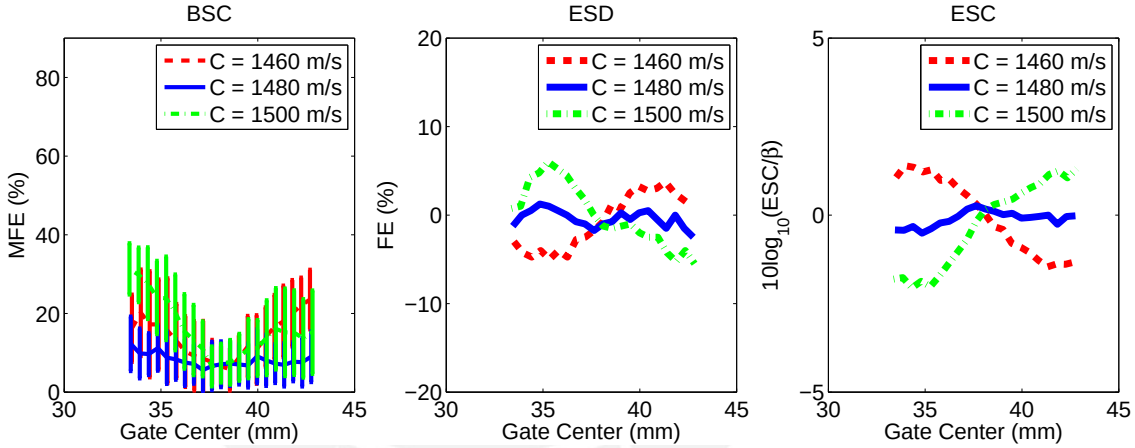

Figure 4.10: Simulation results of the BSC MFE and ESD/ESC FEs for the 10 MHz, f/3 transducer with a 1480 m/s sound speed. The sound speed assumed when calculating the BSCs was set to 1460 m/s (dash), 1480 m/s (solid) and 1500 m/s(dash-dot) in order to assess the robustness of the method.

positive or a negative slope respectively, and when the assumed sound speed is less or more than the real sound speed the ESCs estimates have a negative or a positive slope respectivly. When the assumed values are closer or equal to the real values the slope is close to zero. The same behavior can be observed in all the simulation results. In [33] an assessment of the attenuation estimation when there exists a mismatch in the sound speed when using a reference phantom compensation method was presented. The study showed similar results for small variations respect to the real value of the sound speed. It remains to be studied if the behavior of the QUS curves as a function of depth can be exploited to estimate tissue parameters such as the sound speed.

For the case of the 10 MHz f/2 transducer it can be observed that the error of the ESD and ESC estimation is about 10% and 3 dB greater respectively than for the f/1.5 and f/3 transducers when an error of 1% of the actual value of the focus or the sound speed is introduced. This behavior is directly related to the ratio between the induced location errors and the extent of the focal region (A_D). The 10 MHz f/2 transducer have a focal depth of 50.8 mm and a focal region length of about 28λ, therefore an error of even 1% in the exact position of the focus or in the sound speed will have a greater impact than the one presented with the f/1.5 (with a focal depth of 19.05 mm and a focal region of 15.75λ) or with the f/3 transducer (with a focal depth of 38.1 mm and a focal region of 63λ). The relative shift (R_{shift}) of the focus position, when an error of 1% is introduced, respect to the focal region length using

$$R_{shift} = \frac{0.01(F)}{A_D} \times 100\% \tag{4.8}$$

is about 12% for the f/2 transducer, while is 8% and 4% for the f/1.5 and f/3 transducer respectively.

For a visual demonstration of what has been stated before, another simulation with the 10 MHz f/2 transducer but now introducing a mismatch of just 0.2 mm (relative shift of about 4% of the focal region) in the position of the focus was performed. The result is presented in Figure 4.11.

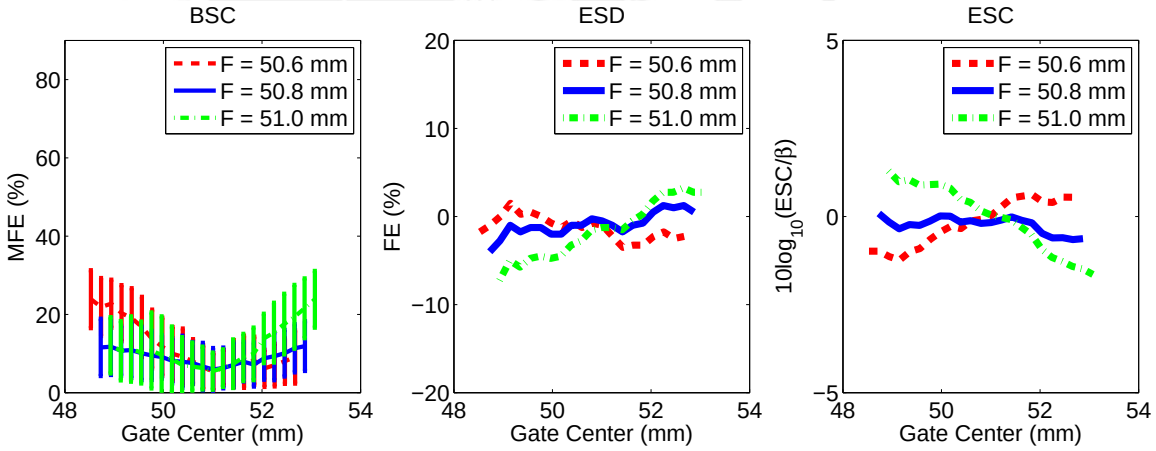

Figure 4.11: Simulation results of the BSC MFE and ESD/ESC FEs for the 10 MHz, f/2 transducer with a 50.8 mm focus. The focus assumed when calculating the BSCs was set to 50.6 mm (dash), 50.8 mm (solid) and 51.0 mm (dash-dot).

This result clearly show the reduction of the ESD and ESC estimation error, in a range comparable to the error obtained for the f/1.5 and f/3 transducers. In addition, this result shows that a relative error in the real position of the transducer focus or in the sound speed will have a greater impact if the transducer focal depth is larger. In general, any of these errors will have a greater impact on QUS images from deeper depths.

4.3.4 Experiments along the transducer focal region

To verify the results of the simulations, the same process were repeated using experimental data. Figs. 4.12-4.14 shows the results for all the 10 MHz experimental transducers presented in Table 4.2 while changing the assumed position of the focus. These results exhibit a very similar behavior to what was observed in simulations, i.e., the performance of QUS estimation may be affected by very small perturbations in the assumed focal distance.

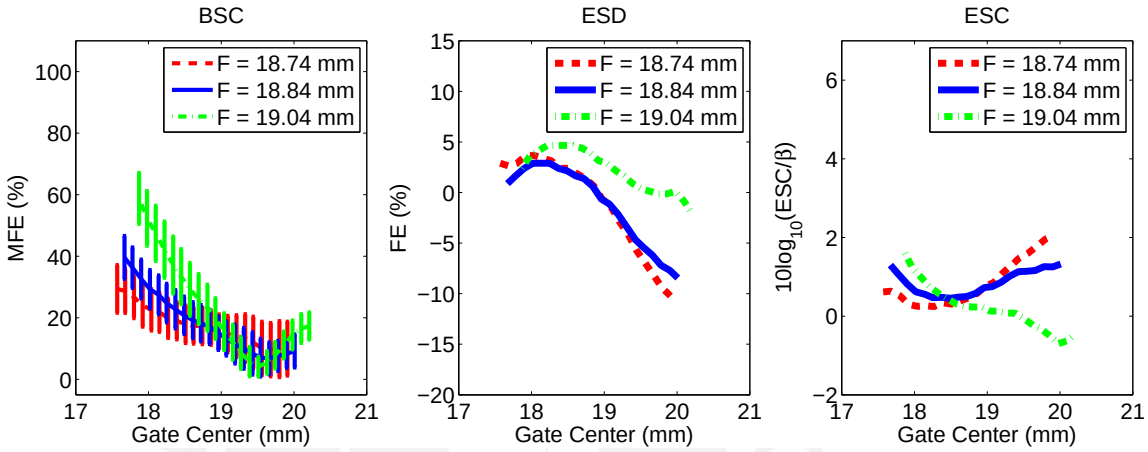

Figure 4.12: Experimental results of the BSC MFE and ESD/ESC FEs for the 10 MHz, f/1.5 transducer. The focus assumed when calculating the BSCs was set to 18.74 mm (dash), 18.84 mm (solid) and 19.04 mm (dash-dot) in order to assess the robustness of the method.

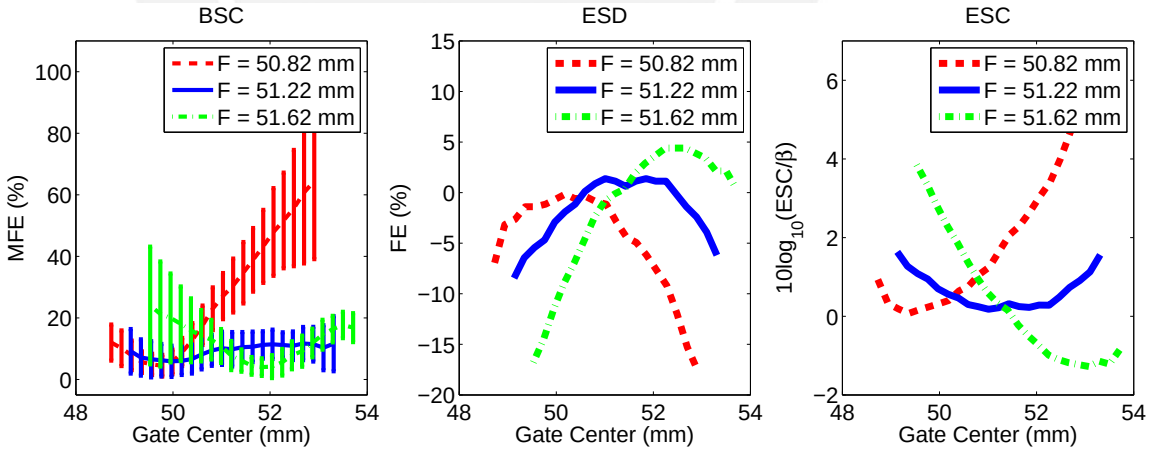

Figure 4.13: Experimental results of the BSC MFE and ESD/ESC FEs for the 10 MHz, f/2 transducer. The focus assumed when calculating the BSCs was set to 50.82 mm (dash), 51.22 mm (solid) and 51.62 mm (dash-dot) in order to assess the robustness of the method.

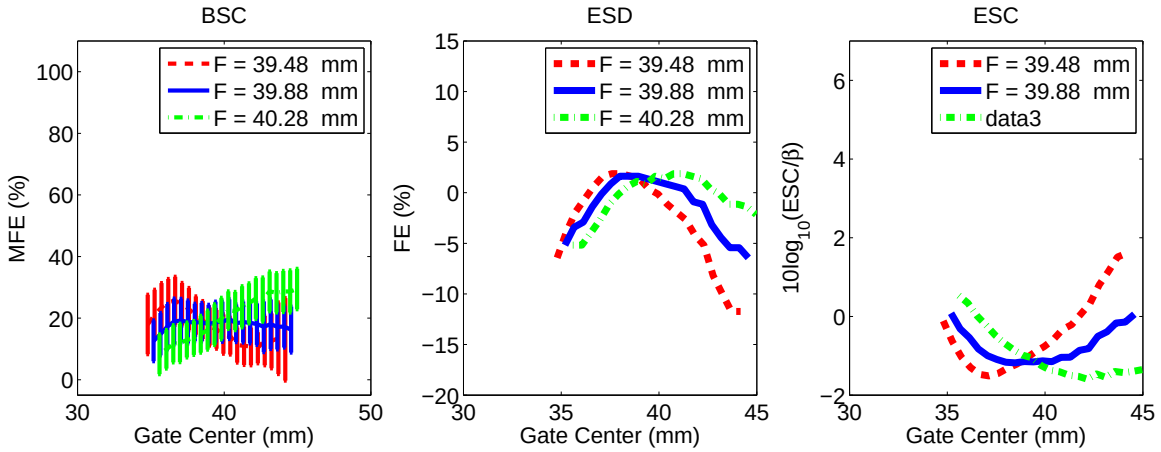

Figure 4.14: Experimental results of the BSC MFE and ESD/ESC FEs for the 10 MHz, f/3 transducer. The focus assumed when calculating the BSCs was set to 39.48 mm (dash), 39.88 mm (solid) and 40.28 mm (dash-dot)) in order to assess the robustness of the method.

The results for the 10 MHz experimental transducers, but now assuming different sound speeds are presented in Figs. 4.15-4.17. These results also shown the same behavior for the slope of the ESCs curves reported before for the simulations.

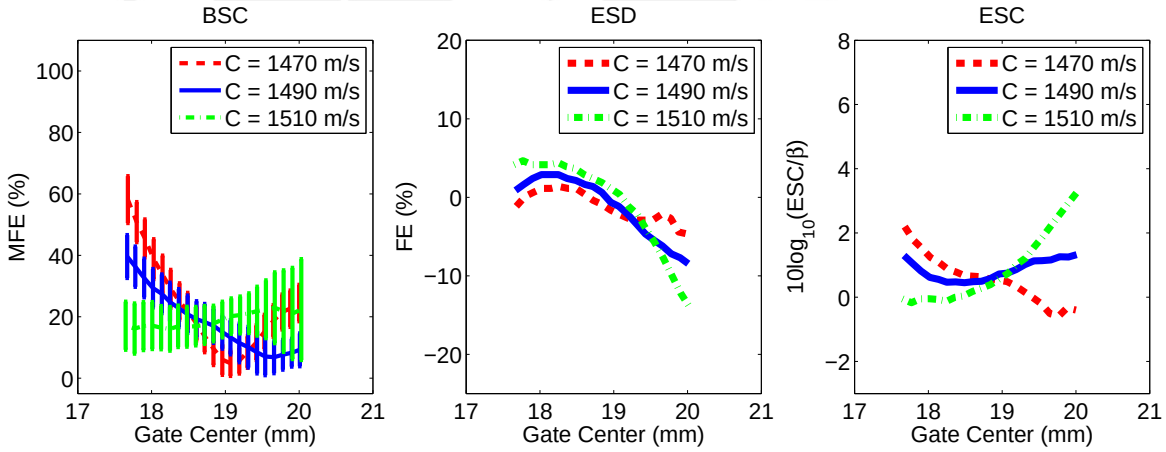

Figure 4.15: Experimental results of the BSC MFE and ESD/ESC FEs for the 10 MHz, f/1.5 transducer. The sound speed assumed when calculating the BSCs was set to 1470 m/s (dash), 1490 m/s (solid) and 1510 m/s(dash-dot) in order to assess the robustness of the method.

It can be observed that although in the average the experimental results present a similar behavior that the simulations, in some cases the errors are more severe than in the simulations. These discrepancies can be potentially due errors in modeling the transducer geometry, errors in the theoretical BSC, attenuation compensation problems, and noise effects.

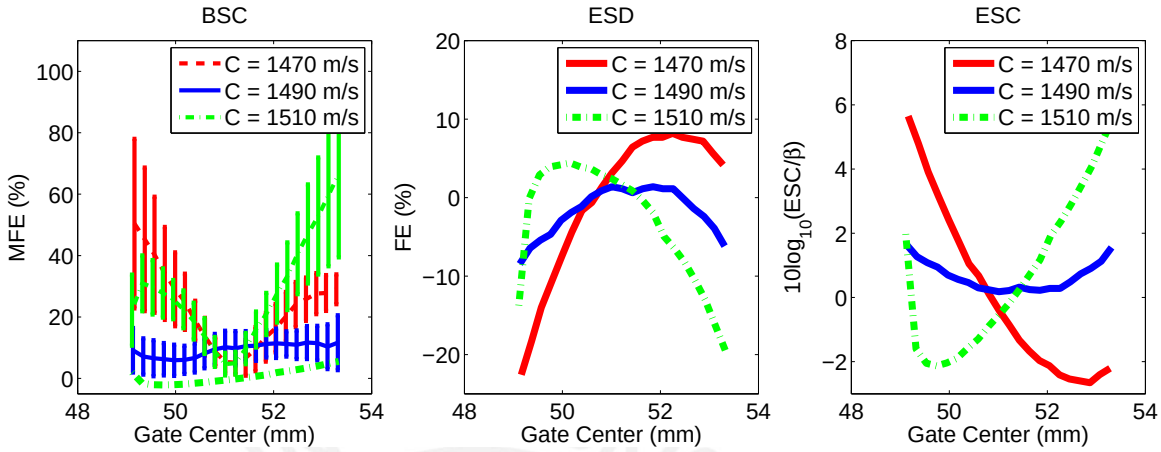

Figure 4.16: Experimental results of the BSC MFE and ESD/ESC FEs for the 10 MHz, f/2 transducer. The sound speed assumed when calculating the BSCs was set to 1470 m/s (dash), 1490 m/s (solid) and 1510 m/s(dash-dot) in order to assess the robustness of the method.

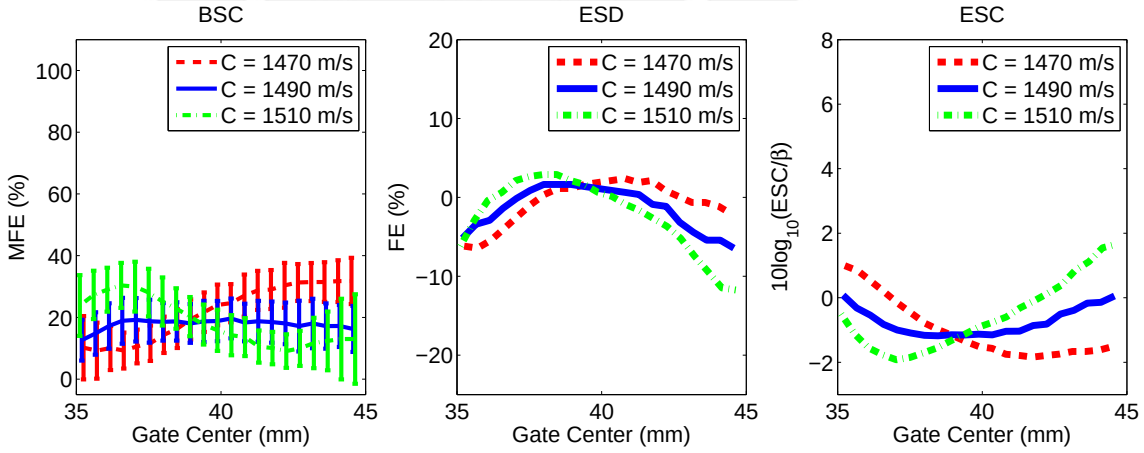

Figure 4.17: Experimental results of the BSC MFE and ESD/ESC FEs for the 10 MHz, f/3 transducer. The sound speed assumed when calculating the BSCs was set to 1470 m/s (dash), 1490 m/s (solid) and 1510 m/s(dash-dot) in order to assess the robustness of the method.

4.4 Conclusions

The presented results suggest that significant improvements in the accuracy of BSC estimation with highly focused transducers can be achieved by using Chen's general model instead of weakly focused transducer formulations.

By improving the BSC estimates the QUS parameters (ESD and ESC) derived from BSCs also present significant improvements based on the FE results. These improvements were not limited to ROIs centered around the transducer focus, but in general better estimates were obtained for ROIs throughout the transducer focal region, allowing to produce better QUS images as shown in the results.

It is important to assess how significant an error of even 1% can be in parameteres as the exact position of the transducer focus and the sound speed. For this, induced errors effects were evaluated and some negatives effects were noticed even with these small errors. Related effects have been reported in other studies, in particular for attenuation estimation [33], where small errors in the sound speed can degrade the attenuation measurements. Other works have showed that the ESC estimation usually have an error of about 2-3dB and an ESD error around 2-10% [2, 34], also the diference between a healthy and a cancerogenic tissue ESD is about 300-500% and the ESC diference is of about 20-30dB [7] indicating that the results obtained can still be used for characterizing tissues.

Chapter 5

Conclusions

In this work, the accuracy of the BSC estimation when using highly focused transducers was evaluated. A theoretical model was developed for estimating BSCs using the FIELD II [19] simulation software, by adapting the model for compensating diffraction effects proposed in [1]. The reliability of the model was assessed, by calculating the MFE between the theoretical and estimated BSC curves using weakly focused transducers. Then calculating the MFE between the theoretical and estimated BSCs curves using highly focused transducers, obtaining MFE values of less than 12% for both cases.

Through simulations, the effectiveness of the CM for estimating accurate BSCs throughout the focal region was evaluated. When the CAM was used at the focus for three highly focused simulated transducers the MFEs varied between 14% and 57%, and were below 10% when the CM was used for the same transducers. This shows a great improvement on the BSC estimates. Moreover, the use of the CM results in MFE values of 15% or less when using information coming from all the focal region and not just from around the transducer focus.

The simulation results were verified using experimental data for estimating BSCs using the CM both from ROIs centered at the focus and throughout the focal region. The experimental results showed the same behavior as the simulations, with better estimates when using the CM for highly focused transducers. Nevertheless, the reductions on the MFEs were not as large as the ones obtained in simulations, potentially because of errors in modeling the transducer geometry, errors in the assumed theoretical BSC, and noise effects. Regardless, the results support advocating for the use of CM when estimating BSCs instead of the CAM for highly focused transducers.

Through simulations, the accuracy of the estimates of the QUS parameters (ESD and ESC) produced using the CM for synthesize BSCs both from around the focus and throughout the focal region was evaluated. When the CM was used for ROIs centered at several positions around the focal region for three highly focused simulated transducers the FEs for the ESD estimates varied between -5% and 2%. For the ESC estimates a decibel scale was used. When the CM was applied, the relation between the estimated and expected values varied between -0.5dB and 1dB. These results showed that the QUS parameter estimation can be highly improved when

using the CM. The improvement is much more notorious for the case of the ESC estimates. These improvements were not limited to ROIs centered at the transducer focus, but in general better estimates were obtained for ROIs throughout the transducer -6-dB focal region, allowing to produce better QUS images as shown in the results.

The simulation results were verified using experimental data for estimating the QUS parameters from the BSCs using the CM. The experimental results showed again the same behavior as the simulations, with better estimates when using the CM for highly focused transducers.

The robustness of the method when using highly focused transducers to uncertainties in parameters like the sound speed and the exact position of the transducer focus was assessed. BSCs were estimated from synthetic data produced using a given sound speed and focus but assuming values that differ slightly to the given ones. The results showed that although on the average the CM provides accurate QUS estimates, the performance of the CM may degrade significantly when the assumed focus location or the sound speed is off even by 1% of its true value. The ESD estimates may degrade up to 20% and the ESC estimates up to 6dB. The degradation is closely related with the relation of the transducer focal depth and focal number. These findings were experimentally validated using data from a physical phantom, which resulted in error curves exhibiting close correlation with the simulation results.

Based on the results it can be concluded that if the appropriate model is used, along with well estimated parameters, highly focused transducers can be used to obtain BSCs and QUS parameters. In addition, better QUS images containing information not restricted to the transducer focus but to the full extention of the transducer focal region can be generated.

Bibliography

[1] Xucai Chen, D. Phillips, K. Q. Schwarz, J. G. Mottley, and K. J. Parker, "The measurement of backscatter coefficient from a broadband pulse-echo system: a new formulation," *IEEE Transactions on Ultrasonics, Ferroelectrics and Frequency Control*, vol. 44, pp. 515 – 525, 1997.

[2] Roberto J. Lavarello, Goutam Ghoshal, and Michael L. Oelze, "On the estimation of backscatter coefficients using single-element focused transducers," *Journal of the Acoustical Society of America*, vol. 129, pp. 2903–2911, 2011.

[3] Gordon S. Kino, *Acoustic Waves: Devices, Imaging, and Analog Signal Processing*, Prentice Hall, 1987.

[4] Zheng Feng Lu, J. A. Zagzebski, and F. T. Lee, "Ultrasound backscatter and attenuation in human liver with diffuse disease," *Ultrasound in Medicine & Biology*, vol. 25, pp. 1047–1054, 1999.

[5] J. A. Zagzebski, Z. F. Lu, and L. X. Yao, "Quantitative ultrasound imaging: in vivo results in normal liver," *Ultrasonic Imaging*, vol. 15, pp. 335–351, 1993.

[6] Z. F. Lu, J. A. Zagzebski, R. T. O'Brien, and H. Steinberg, "Ultrasound attenuation and backscatter in the liver during prednisone administration," *Ultrasound in Medicine and Biology*, vol. 23, pp. 1–8, 1997.

[7] M. L. Oelze, Jr. O'Brien, W. D., J. P. Blue, and J. F. Zachary, "Differentiation and characterization of rat mammary fibroadenomas and 4T1 mouse carcinomas using quantitative ultrasound imaging," *IEEE Transactions on Medical Imaging*, vol. 23, pp. 764–771, 2004.

[8] Michael L. Oelze and James F. Zachary, "Examination of cancer in mouse models using high-frequency quantitative ultrasound," *Ultrasound in Medicine & Biology*, vol. 32, pp. 1639 – 1648, 2006.

[9] K. A. Topp, J. F. Zachary, and W. D O'Brien Jr., "Quantifying B-mode images of in vivo rat mammary tumors by the frequency dependence of backscatter," *Journal of Ultrasound in Medicine*, vol. 20, pp. 605–612, 2001.

[10] B. Barzilai, J. E. Saffitz, J. G. Miller, and B. E. Sobel, "Quantitative ultrasonic characterization of the nature of atherosclerotic plaques in human aorta," *Circulation Research*, vol. 60, pp. 459–463, 1987.

[11] J. W. Mimbs, M. O'Donnell, D. Bauwens, J. W. Miller, and BE Sobel, "The dependence of ultrasonic attenuation and backscatter on collagen content in dog and rabbit hearts," *American Heart Association*, vol. 47, pp. 49–58, 1980.

[12] Keith A. Wear and Brian S. Garra, "Assessment of bone density using ultrasonic backscatter," *Ultrasound in Medicine and Biology*, vol. 24, pp. 689–695, 1998.

[13] M. Soldan, P. C. Silva, A Schanaider, and J. C. Machado, "50 MHz ultrasound characterization of colitis on rats, in vitro," *Proceedings of the IEEE Ultrasonics Symposium*, pp. 1967 – 1970, 2008.

[14] Xiao-Zhou Liu, Xiu-Fen Gong, Dong Zhang, Shi-Gong Ye, and Bing Rui, "Ultrasonic characterization of porcine liver tissue at frequency between 25 to 55 mhz," *World J Gastroenterology*, pp. 2276–2279, 2006.

[15] F. T. Yu, E. Franceschini, B. Chayer, J. K. Armstrong, H. J. Meiselman, and G. Cloutier, "Ultrasonic parametric imaging of erythrocyte aggregation using the structure factor size estimator.," *Biorheology*, pp. 343–363, 2009.

[16] Sebastian Brand, Eike C. Weiss, Robert M. Lemor, and Michael C. Kolios, "High frequency ultrasound tissue characterization and acoustic microscopy of intracellular changes," *Ultrasound in Medicine and Biology*, vol. 34, no. 9, pp. 1396 – 1407, 2008.

[17] J. C. Machado and F. S. Foster, "Experimental validation of a diffraction correction model for high frequency measurement of ultrasound backscatter coefficients," *Proceedings of the IEEE Ultrasonics Symposium*, vol. 2, pp. 1869 – 1872, 1998.

[18] Balasundar I. Raju, Kirsty J. Swindells, Salvador Gonzalez, and Mandayam A. Srinivasan, "Quantitative ultrasonic methods for characterization of skin lesions in vivo," *Ultrasound in Medicine & Biology*, vol. 29, pp. 825 – 838, 2003.

[19] J. A. Jensen and N. B. Svendsen., "Calculation of pressure fields from arbitrarily shaped, apodized, and excited ultrasound transducers.," *IEEE Transactions on Ultrasonics, Ferroelectrics and Frequency Control*, pp. 262–267, 1992.

[20] R. K. Saha and M. C. Kolios, "Effects of cell spatial organization and size distribution on ultrasound backscattering," *IEEE Transactions on Ultrasonics, Ferroelectrics and Frequency Control*, vol. 58, pp. 2118–2131, 2011.

[21] Michael L. Oelze and J. William D. OBrien, "Defining optimal axial and lateral resolution for estimating scatterer properties from volumes using ultrasound backscatter.," *Journal of the Acoustical Society of America*, vol. 115, pp. 3226–3234, 2004.

[22] Anthony Gerig, Quan Chen, James Zagzebski, and Tomy Varghese, "Correlation of ultrasonic scatterer size estimates for the statistical analysis and optimization of angular compounding," *The Journal of the Acoustical Society of America*, vol. 116, pp. 1832–1841, 2004.

[23] J. J. Dahl, G. F. Pinton, M. L. Palmeri, V. Agrawal, K. R. Nightingale, and G. E. Trahey, "A parallel tracking method for acoustic radiation force impulse imaging," *IEEE Transactions on Ultrasonics, Ferroelectrics and Frequency Control*, vol. 54, pp. 301–312, 2007.

[24] T. Misaridis and J. A. Jensen, "Use of modulated excitation signals in medical ultrasound. part i: basic concepts and expected benefits," *IEEE Transactions on Ultrasonics, Ferroelectrics and Frequency Control*, vol. 52, pp. 177–191, 2005.

[25] Jr. James J. Faran, "Sound scattering by solid cylinders and spheres," *Journal of the Acoustical Society of America*, vol. 23, no. 4, pp. 405–418, 1951.

[26] Robert Hickling, "Analysis of echoes from a solid elastic sphere in water," *Journal of the Acoustical Society of America*, vol. 34, pp. 1582–1592, 1962.

[27] Keith A. Wear, Timothy A. Stiles, Gary R. Frank, Ernest L. Madsen, Francis Cheng, Ernest J. Feleppa, Christopher S. Hall, Beom Soo Kim, Paul Lee, William D. OBrien, Michael L. Oelze, Balasundar I. Raju, K. Kirk Shung, Thaddeus A. Wilson, and Jian R. Yuan, "Interlaboratory comparison of ultrasonic backscatter coefficient measurements from 2 to 9 mhz," *Journal of Ultrasound in Medicine*, vol. 24, no. 9, pp. 1235–1250, 2005.

[28] Jon N. Marsh, Michael S. Hughes, Christopher S. Hall, Stephen H. Lewis, Rebecca L. Trousil, Gary H. Brandenburger, Harold Levene, and James G. Miller, "Frequency and concentration dependence of the backscatter coefficient of the ultrasound contrast agent albunex," *The Journal of the Acoustical Society of America*, vol. 104, no. 3, pp. 1654–1666, 1998.

[29] Balasundar I. Raju and Mandayam A. Srinivasan, "High-frequency ultrasonic attenuation and backscatter coefficients of in vivo normal human dermis and subcutaneous fat," *Ultrasound in Medicine & Biology*, vol. 27, no. 11, pp. 1543 – 1556, 2001.

[30] Catherine L. Dent, Michael J. Scott, Samuel A. Wickline, and Christopher S. Hall, "High-frequency ultrasound for quantitative characterization of myocardial edema," *Ultrasound in Medicine & Biology*, vol. 26, no. 3, pp. 375 – 384, 2000.

[31] Michael L. Oelze and Jr. William D. OBrien, "Frequency-dependent attenuation-compensation functions for ultrasonic signals backscattered from random media," *Journal of the Acoustical Society of America*, vol. 111, pp. 2308–19, 2002.

[32] S. A. Goss, R. L. Johnston, and F. Dunn, "Comprehensive compilation of empirical ultrasonic properties of mammalian tissues," *The Journal of the Acoustical Society of America*, vol. 64, no. 2, pp. 423–457, 1978.

[33] K. Nam, I. M. Rosado-Mendez, N.C. Rubert, E. L. Madsen, J.A. Zagzebski, and T. J. Hall, "Ultrasound attenuation measurements using a reference phantom with sound speed mismatch.," *Ultrasonic Imaging*, vol. 33, pp. 256–263, 2011.

[34] Kibo Nam, Ivan M. Rosado-Mendez, Lauren A. Wirtzfeld, Viksit Kumar, Ernest L. Madsen, Goutam Ghoshal, Alexander D. Pawlicki, Michael L. Oelze, Roberto J. Lavarello, Timothy A. Bigelow, James A. Zagzebski, Jr. William D. O'Brien, and Timothy J. Hall, "Cross-imaging system comparison of backscatter coefficient estimates from a tissue-mimicking material," *The Journal of the Acoustical Society of America*, vol. 132, pp. 1319–1324, 2012.